RESEARCH DEPARTMENT REPORT SERIES no. 36-2011 ISSN 1749-8775

LOWER SEVERN VALLEY
PILOTING OPTICAL DATING OF TERRACES

SCIENTIFIC DATING REPORT

Phil Toms, Tony Brown, Robin Jackson and Andrew Mann

ARCHAEOLOGICAL SCIENCE

ENGLISH HERITAGE

Research Department Report Series 36-2011

LOWER SEVERN VALLEY

PILOTING OPTICAL DATING OF TERRACES

Phil Toms[1], Tony Brown[2], Robin Jackson[3] and Andrew Mann[3]

NGR:

ISSN 1749-8775

SUMMARY
This study contributes to Stage 2 of the English Heritage project 'Evaluating and Enhancing the Geoarchaeological Resource of the Lower Severn Valley'. It aims to assess the potential of Optical dating of terraces in the project area as part of a prospection toolkit that will increase the effectiveness of archaeological mitigation strategies within the particular environment of the Severn Valley. Twelve samples of sediments associated with terraces were collected from active quarry sites at Frampton, Clifton and Ball Mill. Each yielded sufficient datable mass and signal to generate Optical age estimates. The terrace deposits at Frampton and Clifton formed after the Last Glacial Maximum of Marine Isotope Stage (MIS) 2 and prior to mid MIS 1. Those at Ball Mill were created between MIS 5e and early MIS 4. Most of the age estimates are accompanied by analytical caveats though are on the whole consistent with their relative stratigraphic positions. The occurrence of samples at Frampton and Clifton exhibiting traits of partial bleaching suggests that future Optical dating of terraces 1 and 2 should draw upon single grain approaches to acquire ages more consistent with the burial period. Intrinsic assessment of reliability would also be improved by obtaining at least two samples from each unit to be dated that have distinct dose rates, identified either by profiling before or prioritising after sampling.

CONTRIBUTORS
Dr Phil Toms, Prof Tony Brown, Robin Jackson and Andrew Mann

ACKNOWLEDGEMENTS
This OSL dating programme formed part of the much larger project "Evaluating and Enhancing the Geoarchaeological Resource of the Lower Severn Valley" that was directed by Robin Jackson (Worcestershire Historic Environment and Archaeology Service) with support from Toby Catchpole (Gloucestershire County Council Archaeology Service). The project was funded through the Aggregates Levy Sustainability Fund managed by English Heritage.

ARCHIVE LOCATION
Historic Environment and Archaeology Service, Worcestershire County Council,
Woodbury Building, University of Worcester,
Henwick Grove, Worcester WR2 6AJ

DATE OF INVESTIGATION
2008–10

CONTACT DETAILS
[1]Geochronology Laboratories, Department of Natural and Social Sciences, University of Gloucestershire, Swindon Road, Cheltenham GL50 4AZ. Tel: 01242 714708
Email: ptoms@glos.ac.uk
[2]School of Geography, University of Southampton, University Road, Southampton SO17 1BJ
[3]Worcestershire Historic Environment and Archaeology Service, Woodbury, University of Worcester, Henwick Grove, Worcester WR2 6AJ

CONTENTS

1.0 Introduction 1
2.0 Optical Dating: Mechanisms and Principles 1
3.0 Sample Collection and Preparation 2
4.0 Acquisition and Accuracy of D_e Value 3
4.1 Laboratory factors 3
4.1.1 Feldspar contamination 3
4.1.2 Preheating 4
4.1.3 Irradiation 5
4.1.4 Internal consistency 5
4.2 Environmental factors 5
4.2.1 Incomplete zeroing 5
4.2.2 Pedoturbation 6
5.0 Acquisition and Accuracy of D_r Value 7
6.0 Estimation of Age 8
7.0 Analytical Uncertainty 8
8.0 Intrinsic assessment of reliability 9
9.0 Discussion 10
10.0 References 11
Appendix I: Technical Data for Sample GL08060 23
Appendix II: Technical Data for Sample GL08059 24
Appendix III: Technical Data for Sample GL08057 25
Appendix IV: Technical Data for Sample GL10021 26
Appendix V: Technical Data for Sample GL10022 27
Appendix VI: Technical Data for Sample GL10023 28
Appendix VII: Technical Data for Sample GL10017 29
Appendix VIII: Technical Data for Sample GL10018 30
Appendix IX: Technical Data for Sample GL10024 31
Appendix X: Technical Data for Sample GL10025 32
Appendix XI: Technical Data for Sample GL10027 33
Appendix XII: Technical Data for Sample GL10026 34

1.0 INTRODUCTION

This study contributes to Stage 2 of the English Heritage funded project 'Evaluating and Enhancing the Geoarchaeological Resource of the Lower Severn Valley (Ref: PNUM 5725 PD)'. The Lower Severn Valley remains one of the few major UK valley floors that holds significant aggregate resources. In anticipation of increased aggregate extraction, the overarching aim of the project is to improve methodological approaches and baseline information underpinning strategic planning, individual application decisions and evaluation and mitigation strategies relating to mineral extraction in this area. Stage 2, in part, pilots Optically Stimulated Luminescence (OSL) dating of terraces within the Lower Severn Valley focussing on three active quarries, Frampton, Clifton and Ball Mill (Figs 1–4), and draws on recent research at the University of Gloucestershire (Earle 2009). This report summarises the findings of the initial OSL programme.

2.0 OPTICAL DATING: MECHANISMS AND PRINCIPLES

Upon exposure to ionising radiation, electrons within the crystal lattice of insulating minerals are displaced from their atomic orbits. Whilst this dislocation is momentary for most electrons, a portion of charge is redistributed to meta-stable sites (traps) within the crystal lattice. In the absence of significant optical and thermal stimuli, this charge can be stored for extensive periods. The quantity of charge relocation and storage relates to the magnitude and period of irradiation. When the lattice is optically or thermally stimulated, charge is evicted from traps and may return to a vacant orbit position (hole). Upon recombination with a hole, an electron's energy can be dissipated in the form of light-generating crystal luminescence, providing a measure of dose absorption.

Herein, quartz is segregated for dating. The utility of this minerogenic dosimeter lies in the stability of its datable signal over the mid to late Quaternary period, predicted through isothermal decay studies (eg Smith *et al* 1990; retention lifetime 630Ma at 20°C) and evidenced by optical age estimates concordant with independent chronological controls (eg Murray and Olley 2002). This stability is in contrast to the anomalous fading of comparable signals commonly observed for other ubiquitous sedimentary minerals, such as feldspar and zircon (Wintle 1973; Templer 1985; Spooner 1993).

Optical age estimates of sedimentation (Huntley *et al* 1985) are premised upon reduction of the minerogenic time-dependent signal (Optically Stimulated Luminescence, OSL) to zero through exposure to sunlight and, once buried, signal reformulation by absorption of litho- and cosmogenic radiation. The signal accumulated post-burial acts as a dosimeter recording total dose absorption, converting to a chronometer by estimating the rate of dose absorption quantified through the assay of radioactivity in the surrounding lithology and streaming from the cosmos.

$$\text{Age} = \text{Mean Equivalent Dose } (D_e, \text{Gy}) / \text{Mean Dose Rate } (D_r, \text{Gy.ka}^{-1})$$

Aitken (1998) and Bøtter-Jensen *et al* (2003) offer a detailed review of optical dating.

3.0 SAMPLE COLLECTION AND PREPARATION

A total of 12 samples are reported herein; three collected by Earle (2009; GL08057, GL08058, GL08060) and nine as part of Stage 2 of this project (Table 1). All are conventional sediment samples, located within matrix-supported units composed predominantly of sand and silt collected in daylight from sections by means of opaque plastic tubing (150x45 mm) forced into each face. Each was taken from primary terrace material with the exception of GL08059/GL08060 (Clifton) and GL10024 (Ball Mill), where alluviated and aeolian sediments capping the terrace deposits were sampled, respectively. In order to attain an intrinsic metric of reliability and where possible, two samples were obtained from stratigraphically equivalent units targeting positions likely divergent in dosimetry on the basis of textural and colour differences (see section 8.0). Each sample was wrapped in cellophane and parcel tape in order to preserve moisture content and integrity until ready for laboratory preparation. For each sample, an additional *c* 100g of sediment was collected for laboratory-based assessment of radioactive disequilibrium. The location of each OSL dating sample are shown in Figures 1 to 3.

To preclude optical erosion of the datable signal prior to measurement, all samples were prepared under controlled laboratory illumination provided by Encapsulite RB-10 (red) filters. To isolate that material potentially exposed to daylight during sampling, sediment located within 20mm of each tube-end was removed.

The remaining sample was dried and then sieved. Quartz within the fine sand (125–180, 180–250μm) or fine silt (5–15μm) fraction was segregated, based on modal grain size (Table 1). Samples were then subjected to acid and alkaline digestion (10% HCl, 15% H_2O_2) to attain removal of carbonate and organic components respectively.

For fine sand fractions, a further acid digestion in HF (40%, 60 mins) was used to etch the outer 10–15 μm layer affected by α radiation and degrade each samples' feldspar content. During HF treatment, continuous magnetic stirring was used to effect isotropic etching of grains. 10% HCl was then added to remove acid soluble fluorides. Each sample was dried, resieved and quartz isolated from the remaining heavy mineral fraction using a sodium polytungstate density separation at 2.68g.cm^{-3}. Twelve multi-grain aliquots (*c* 3–6 mg) of quartz from each sample were then mounted on aluminium discs for determination of D_e values.

Fine silt sized quartz, along with other mineral grains of varying density and size, was extracted by sample sedimentation in acetone (<15μm in 2min 20s, >5μm in 21mins at 20°C). Feldspars and amorphous silica were then removed from this fraction through acid digestion (35% H_2SiF_6 for 2 weeks, Jackson *et al* 1976; Berger *et al* 1980). Following addition of 10% HCl to remove acid soluble fluorides, grains degraded to <5μm as a result of acid treatment were removed by acetone sedimentation. 6 aliquots (*c* 1.5mg) were then mounted on aluminium discs for D_e evaluation.

All drying was conducted at 40°C to prevent thermal erosion of the signal. All acids and alkalis were Analar grade. All dilutions (removing toxic-corrosive and non-minerogenic luminescence-bearing substances) were conducted with distilled water to prevent signal contamination by extraneous particles.

4.0 ACQUISITION AND ACCURACY OF D_E VALUE

All minerals naturally exhibit marked inter-sample variability in luminescence per unit dose (sensitivity). Therefore, the estimation of D_e acquired since burial requires calibration of the natural signal using known amounts of laboratory dose. D_e values were quantified using a single-aliquot regenerative-dose (SAR) protocol (Murray and Wintle 2000; 2003) facilitated by a Risø TL-DA-15 irradiation-stimulation-detection system (Markey *et al* 1997; Bøtter-Jensen *et al* 1999). Within this apparatus, optical signal stimulation of each sample was provided by one of two light sources: an assembly of blue diodes (five packs of six Nichia NSPB500S), filtered to 470 ±80nm, conveying 15mW.cm^{-2} using a 3mm Schott GG420 positioned in front of each diode pack. Infrared (IR) stimulation, provided by 6 IR diodes (Telefunken TSHA 6203) stimulating at 875 ±80nm delivering ~5mW.cm^{-2}, was used to indicate the presence of contaminant feldspars (Hütt *et al* 1988). Stimulated photon emissions from quartz aliquots are in the ultraviolet (UV) range and were filtered from stimulating photons by 7.5mm HOYA U-340 glass and detected by an EMI 9235QA photomultiplier fitted with a blue-green sensitive bialkali photocathode. Aliquot irradiation was conducted using a 1.48GBq ^{90}Sr/^{90}Y β source calibrated for multi-grain aliquots of each isolated quartz fraction against the 'Hotspot 800' ^{60}Co γ source located at the National Physical Laboratory (NPL), UK.

SAR by definition evaluates D_e through measuring the natural signal (Fig 1 in each Appendix) of a single aliquot and then regenerating that aliquot's signal by using known laboratory doses to enable calibration. For each aliquot, five different regenerative doses were administered, so as to image dose response. D_e values for each aliquot were then interpolated, and associated counting and fitting errors calculated, by way of linear or exponential regression (Fig 1 in each Appendix). Weighted (geometric) mean D_e values were calculated from the 12 aliquots using the central age model outlined by Galbraith *et al* (1999), and are quoted at 1σ confidence. The accuracy with which D_e equates to total absorbed dose and that dose absorbed since burial is assessed. The former can be considered a function of laboratory factors, the latter, one of environmental issues. Diagnostics were deployed to estimate the influence of these factors and criteria instituted to optimise the accuracy of D_e values.

4.1 Laboratory factors

4.1.1 Feldspar contamination

The propensity of feldspar signals to fade and underestimate age, coupled with their higher sensitivity relative to quartz, makes it imperative to qualify feldspar contamination.

At room temperature, feldspars generate a signal (IRSL) upon exposure to IR, whereas quartz does not. The signal from feldspars contributing to OSL can be depleted by prior exposure to IR. For all aliquots the contribution of any remaining feldspars was estimated from the OSL IR depletion ratio (Duller 2003). If the addition to OSL by feldspars is insignificant, then the repeat dose ratio of OSL to post-IR OSL should be statistically consistent with unity (Figs 1 and 6 in each Appendix). Any aliquots that did not fulfil this criterion were rejected. The source of feldspar contamination is rarely rooted in sample preparation; it predominantly results from the occurrence of feldspars as inclusions within quartz.

4.1.2 Preheating

Preheating aliquots between irradiation and optical stimulation is necessary to ensure comparability between natural and laboratory-induced signals. However, the multiple irradiation and preheating steps that are required to define single-aliquot regenerative-dose response leads to signal sensitisation, rendering calibration of the natural signal inaccurate. The SAR protocol (Murray and Wintle 2000; 2003) enables this sensitisation to be monitored and corrected using a test dose, here set at *c* 20Gy preheated to 220°C for 10s, to track signal sensitivity between irradiation-preheat steps. However, the accuracy of sensitisation correction for both natural and laboratory signals can be preheat-dependent. Three diagnostics were used to assess the optimal preheat temperature for accurate correction and calibration.

Irradiation-preheat cycling (Fig 2 in each Appendix) quantifies the preheat dependence of sensitisation correction for laboratory-induced signals. If sensitisation is accurately corrected, then the same regenerative dose should yield an equivalent sensitivity-corrected value, irrespective of the number of times it is applied and its associated signal measured. The ratio of subsequent to initial corrected regenerative-dose signals should be statistically concordant with unity. Alternatively, this ratio may differ from unity yet attain consistency after one or more cycles, evidencing that accurate sensitivity correction exists if the sample is primed by irradiation-preheat cycles. For this diagnostic, 18 aliquots were divided into sets of three, and assigned a 10s preheat between 180°C and 280°C.

D_e preheat dependence (Fig 3 in each Appendix) quantifies the combined effects of thermal transfer and sensitisation on the natural signal. Insignificant adjustment in D_e values in response to differing preheats may reflect limited influence of these effects. Samples generating D_e values <10Gy and exhibiting a systematic, statistically significant adjustment in D_e value with increasing preheat temperature may indicate the presence of significant thermal transfer; in such instances low temperature (<220°C) preheats may provide the apposite measure of D_e. For this diagnostic, the D_e value of each of the same 18 aliquots and their assigned preheat was assessed.

Dose recovery (Fig 4 in each Appendix) attempts to replicate the above diagnostic, yet provide improved resolution of thermal effects through removal of variability induced by

heterogeneous dose absorption in the environment, using a precise laboratory dose to simulate natural dose. The ratio between the applied dose and recovered D_e value should be statistically concordant with unity. For this diagnostic, a further six aliquots were each assigned a 10s preheat between 180°C and 280°C.

That preheat treatment fulfilling the criterion of accuracy for all three diagnostics was selected to refine the final D_e value from a further nine aliquots. Further thermal treatments, prescribed by Murray and Wintle (2000; 2003), were applied to optimise accuracy and precision. Optical stimulation occurred at 125°C, in order to minimise effects associated with photo-transferred thermoluminescence and maximise signal-to-noise ratios. Inter-cycle optical stimulation was conducted at 280°C to minimise recuperation.

4.1.3 Irradiation

For all samples having D_e values in excess of 100Gy, matters of signal saturation and laboratory irradiation effects are of concern. As regards the former, the rate of signal accumulation generally adheres to a saturating exponential form, and it is this that limits the precision and accuracy of D_e values for samples having absorbed large doses. For such samples, the functional range of D_e interpolation is defined from log-linear plots of dose response. Within these plots, the maximum D_e value is delimited by the cessation of statistically significant increases in signal response. However, in this study no D_e value exceeded 100Gy.

4.1.4 Internal consistency

Quasi-radial plots (*cf* Galbraith 1990) are used to illustrate inter-aliquot D_e variability for natural, repeat regenerative-dose and OSL to post-IR OSL signals (Figs 4–6, respectively, in each Appendix). D_e values are standardised relative to the central D_e value for natural signals and applied dose for regenerated signals. D_e values are described as overdispersed when >5% lie beyond $\pm 2\sigma$ of the standardising value; resulting from a heterogeneous absorption of burial dose and/or response to the SAR protocol. For multi-grain aliquots, overdispersion of natural signals does not necessarily imply inaccuracy. However where overdispersion is observed for regenerated signals, the age estimate from that sample should be accepted tentatively.

4.2 Environmental factors

4.2.1 Incomplete zeroing

Post-burial OSL signals residual of pre-burial dose absorption can result where pre-burial sunlight exposure is limited in spectrum, intensity, and/or period, leading to age over-estimation. This effect is particularly acute for material eroded and redeposited sub-

aqueously (Olley *et al* 1998, 1999; Wallinga 2002) and exposed to a burial dose of less than c 20Gy (eg Olley et al 2004) and can have some influence in sub-aerial contexts, but is rarely of consequence where aerial transport has occurred. Within single-aliquot regenerative-dose optical dating, there are two diagnostics of partial resetting (or bleaching); signal analysis (Agersnap Larsen *et al* 2000; Bailey *et al* 2003) and inter-aliquot D_e distribution studies (Murray *et al* 1995).

Within this study, signal analysis is used to quantify the change in D_e value with respect to optical stimulation time for multi-grain aliquots. This exploits the existence of traps within minerogenic dosimeters that bleach with different efficiency for a given wavelength of light to verify partial bleaching. D_e (t) plots (Fig 7 in each Appendix; Bailey *et al* 2003) are constructed from separate integrals of signal decay as laboratory optical stimulation progresses. A statistically significant increase in natural D_e (t) is indicative of partial bleaching, assuming three conditions are fulfilled. Firstly, that a statistically significant increase in D_e (t) is observed when partial bleaching is simulated within the laboratory. Secondly, that there is no significant rise in D_e (t) when full bleaching is simulated. Finally, there should be no significant augmentation in D_e (t) when zero dose is simulated. Where partial bleaching is detected, the age derived from the sample should be considered a maximum estimate only. However, the utility of signal analysis is strongly dependent upon a sample's pre-burial experience of sunlight's spectrum and its residual to post-burial signal ratio. Given that, in the majority of cases, the spectral exposure history of a deposit is uncertain, the absence of an increase in natural D_e (t) does not necessarily testify to the absence of partial bleaching.

4.2.2 Pedoturbation

The accuracy of sedimentation ages can further be controlled by post-burial trans-strata grain movements forced by pedo- or cryoturbation. Berger (2003) contends that pedogenesis prompts a reduction in the apparent sedimentation age of parent material through bioturbation and illuviation of younger material from above, and/or by biological recycling and resetting of the datable signal of surface material. Berger (2003) proposes that the chronological products of this remobilisation are A-horizon age estimates reflecting the cessation of pedogenic activity, Bc/C-horizon ages delimiting the maximum age for the initiation of pedogenesis, with estimates obtained from Bt-horizons providing an intermediate age 'close to the age of cessation of soil development'. Singhvi *et al* (2001), in contrast, suggest that B and C-horizons closely approximate the age of the parent material, the A-horizon, that of the 'soil forming episode'. At present there is no post-sampling mechanism for the direct detection of, and correction for, post-burial sediment remobilisation. However, intervals of palaeosol evolution can be delimited by a maximum age derived from parent material and a minimum age obtained from a unit overlying the palaeosol. Inaccuracy forced by cryoturbation may be bidirectional, heaving older material upwards or drawing younger material downwards into the level to be dated. Cryogenic deformation of matrix-supported material is, typically, visible; sampling of such cryogenically-disturbed sediments can be avoided. Though pedo- and cryoturbated

sediments were observed during this study, none of the sediment samples were located close to such deposits.

5.0 ACQUISITION AND ACCURACY OF D_R VALUE

Lithogenic D_r values were defined through measurement of U, Th, and K radionuclide concentration, and conversion of these quantities into α, β, and γ D_r values (Table 1). α and β contributions were estimated from sub-samples by laboratory-based γ spectrometry using an Ortec GEM-S high purity Ge coaxial detector system, calibrated using certified reference materials supplied by CANMET. γ dose rates were estimated from *in-situ* NaI gamma spectrometry. *In-situ* measurements were conducted using an EG&G μNomad portable NaI gamma spectrometer (calibrated using the block standards at RLAHA, University of Oxford); these reduce uncertainty relating to potential heterogeneity in the γ dose field surrounding each sample. The level of U disequilibrium was estimated by laboratory-based Ge γ spectrometry. Estimates of radionuclide concentration were converted into D_r values (Adamiec and Aitken 1998), accounting for D_r modulation forced by grain size (Mejdahl 1979), present moisture content (Zimmerman 1971), and, given that D_e values were generated from 5–15μm quartz, reduced signal sensitivity to α radiation (a-value 0.050 ±0.002; Toms unpubl data). Cosmogenic D_r values are calculated on the basis of sample depth, geographical position, and matrix density (Prescott and Hutton 1994).

The spatiotemporal validity of D_r values can be considered as five variables. Firstly, age estimates devoid of *in-situ* γ spectrometry data should be accepted tentatively if the sampled unit is heterogeneous in texture or if the sample is located within 0.3m of strata consisting of differing texture and/or mineralogy. However, where samples are obtained throughout a vertical profile, consistent values of γ D_r based solely on laboratory measurements may evidence the homogeneity of the γ field and hence accuracy of γ D_r values. Secondly, disequilibrium can force temporal instability in U and Th emissions. The impact of this infrequent phenomenon (Olley *et al* 1996) upon age estimates is usually insignificant, given their associated margins of error. However, for samples where this effect is pronounced (>50% disequilibrium between ^{238}U and ^{226}Ra; Fig 8 in each Appendix), the resulting age estimates should be accepted tentatively. Thirdly, pedogenically-induced variations in matrix composition of B and C-horizons, such as radionuclide and/or mineral remobilisation, may alter the rate of energy emission and/or absorption. If D_r is invariant through a dated profile and samples encompass primary parent material, then element mobility is probably limited in effect. Fourthly, spatiotemporal deviations from present moisture content are difficult to assess directly, requiring knowledge of the magnitude and timing of differing contents. However, the maximum influence of moisture content variations can be delimited by recalculating D_r for minimum (zero) and maximum (saturation) content. Finally, temporal alteration in the thickness of overburden alters cosmic D_r values. Cosmic D_r often forms a negligible portion of total D_r. It is possible to quantify the maximum influence of overburden flux by recalculating D_r for minimum (zero) and maximum (surface sample) cosmic D_r.

6.0 ESTIMATION OF AGE

Age estimates reported in Table 1 provide an estimate of sediment burial period based on mean D_e and D_r values and their associated analytical uncertainties. Uncertainty in age estimates is reported as a product of systematic and experimental errors, with the magnitude of experimental errors alone shown in parentheses (Table 1). Probability distributions indicate the inter-aliquot variability in age (Fig 9 in each Appendix). The maximum influence of temporal variations in D_r forced by minima-maxima variation in moisture content and overburden thickness is illustrated in Figure 8 in each Appendix. Where uncertainty in these parameters exists, this age range may prove instructive, but the combined extremes represented should not be construed as preferred age estimates.

7.0 ANALYTICAL UNCERTAINTY

All errors are based upon analytical uncertainty and quoted at 1σ confidence. Error calculations account for the propagation of systematic and/or experimental (random) errors associated with D_e and D_r values.

For D_e values, systematic errors are confined to laboratory β source calibration. Uncertainty in this respect is that combined from the delivery of the calibrating γ dose (1.2%; NPL pers comm), the conversion of this dose for SiO_2 using the respective mass energy-absorption coefficient (2%; Hubbell 1982) and experimental error, totalling 3.5%. Mass attenuation and Bremsstrahlung losses during γ dose delivery are considered negligible. Experimental errors relate to D_e interpolation using sensitisation-corrected dose responses. Natural and regenerated sensitisation corrected dose points (S_i) are quantified by

$$S_i = (D_i - x.L_i) / (d_i - x.L_i) \qquad \text{Eq. 1}$$

where D_i = Natural or regenerated OSL, initial 0.2s

L_i = Background natural or regenerated OSL, final 5s

d_i = Test dose OSL, initial 0.2s

x = Scaling factor, 0.08

The error on each signal parameter is based on counting statistics, reflected by the square-root of measured values. The propagation of these errors within Eq. 1 generating σS_i follows the general formula given in Eq. 2. σS_i are then used to define fitting and interpolation errors within linear or exponential regressions (Green and Margerison 1978; Ixaru *et al* 2004).

For D_r values, systematic errors accommodate uncertainty in radionuclide conversion factors (5%), β attenuation coefficients (5%), a-value (4%; derived from a systematic α source uncertainty of 3.5% and experimental error), matrix density (0.20 $g.cm^{-3}$), vertical thickness of sampled section (specific to sample collection device), saturation moisture content (3%), moisture content attenuation (2%), burial moisture content (25% relative, unless direct evidence exists of the magnitude and period of differing content), NaI gamma spectrometer calibration (3%) and/or NAA/ICP-MS (2%). Experimental errors are associated with radionuclide quantification for each sample by gamma spectrometry and/or NAA/ICP-MS.

The propagation of these errors through to age calculation is quantified using the expression,

$$\sigma y\ (\delta y/\delta x) = (\Sigma\ ((\delta y/\delta x_n).\sigma x_n)^2)^{1/2} \qquad \text{Eq. 2}$$

where y is a value equivalent to that function comprising terms x_n and where δy and δx_n are associated uncertainties.

Errors on age estimates are presented as combined systematic and experimental errors and experimental errors alone. The former (combined) error should be considered when comparing luminescence ages herein with independent chronometric controls. The latter assumes systematic errors are common to luminescence age estimates generated by means equal to those detailed herein and enable direct comparison with those estimates.

8.0 INTRINSIC ASSESSMENT OF RELIABILITY

Intrinsic measures of reliability in Luminescence dating are based on analytical acceptability and inference. Table 2 details the analytical acceptability of age estimates evolved in this study, drawn principally from diagnostics illustrated in Figures 1 to 8 and detailed in sections 4.0 to 5.0. Inference of reliability comes from the level of intra-site stratigraphic consistency and the convergence of age estimates from stratigraphically equivalent units of divergent dosimetry (Toms *et al* 2005; 2008). Hierarchically, comparable ages derived from stratigraphically equivalent units of differing D_r supersede analytical acceptability even where the latter is questionable.

At Frampton two samples were taken from the same unit, owing to the limited exposure of sediments at this site. The age of GL10017 is significantly older than GL10018. Figure 7 for the former sample indicates the occurrence of partial bleaching and thus an overestimation of age. All age estimates from Clifton are consistent with their relative stratigraphic position. Three of the five samples (GL08057, GL08059, GL10021) exhibit traits of partial bleaching. Two samples (GL10021 and GL10022) were taken from an equivalent stratigraphic unit at this site with the intention of targeting areas of differing D_r. These samples produced coeval age estimates despite having differing analytical caveats. However the dosimetry for each sample proved indistinguishable, precluding the

assessment of reliability based on divergent dosimetry. The age estimates generated from Ball Mill are, statistically, consistent with their relative stratigraphic positions. Two samples (GL10025 and GL10026) exhibited moderate U disequilibrium, but the consistency of their age estimates with those devoid of this effect suggests a negligible impact on accuracy.

9.0 DISCUSSION

From this pilot study, sediments associated with terraces in the Lower Severn Valley have sufficient datable mass and signal to produce Optical age estimates. The probable age of the terrace sediments at Frampton is 9.7 ±1.2ka (late MIS 2 to early MIS 1). The terrace deposits at Clifton formed between 18 and 5.5ka (late MIS 2 to mid MIS 1), with subsequent alluviation recorded between 2.8 and 0.7ka. At Ball Mill, sedimentation of terrace material occurred between 122 and 71ka (MIS 5e to early MIS 4).

All samples, with the exception of GL08060, are accompanied by analytical caveats. These alone do not warrant rejection of the associated age estimates. However, the occurrence of partially bleached sediments at Frampton and Clifton is consistent with previous studies of sub-aqueous sediments exposed to less than *c* 20 Gy during burial (Olley *et al* 1998; 1999; 2004; Wallinga 2002). Correction of the resulting age overestimation may be possible through inter-aliquot D_e distribution studies. Such analyses use aliquots of single sand grains to quantify inter-grain D_e distribution. At present, it is contended that asymmetric inter-grain D_e distributions are symptomatic of partial bleaching and/or pedoturbation (Murray *et al* 1995; Olley *et al* 1999; 2004; Bateman *et al* 2003). For partial bleaching at least, it is further contended that the D_e acquired during burial is located in the minimum region of such ranges reflecting fully or well-bleached grains. Therefore, a single grain approach to further Optical dating of terraces 1 and 2 in the Lower Severn Valley is advocated.

As a pilot study, the opportunity to pursue multiple samples of divergent dosimetry from equivalent stratigraphic units is limited. In the instances where two samples were obtained from the same unit (Frampton and Clifton), the D_r values proved to be indistinguishable. It is recommended that any further Optical dating should attempt to either profile dosimetry within a unit prior to sampling or take multiple samples from the same unit, prioritising for analysis those with significantly different D_r values.

10.0 REFERENCES

Adamiec, G, and Aitken, M J, 1998 Dose-rate conversion factors: new data, *Ancient TL*, **16**, 37–50

Agersnap-Larsen, N, Bulur, E, Bøtter-Jensen, L, and McKeever, S W S, 2000 Use of the LM-OSL technique for the detection of partial bleaching in quartz, *Radiation Measurements*, **32**, 419–25

Aitken, M J, 1998 *An introduction to optical dating: the dating of Quaternary sediments by the use of photon-stimulated luminescence*, Oxford (Oxford University Press)

Bailey, R M, Singarayer, J S, Ward, S, and Stokes, S, 2003 Identification of partial resetting using D_e as a function of illumination time, *Radiation Measurements*, **37**, 511–8

Banerjee, D, Murray, A S, Bøtter-Jensen, L, and Lang, A, 2001 Equivalent dose estimation using a single aliquot of polymineral fine grains, *Radiation Measurements*, **33**, 73–94

Bateman, M D, Frederick, C D, Jaiswal, M K, Singhvi, A K, 2003 Investigations into the potential effects of pedoturbation on luminescence dating, *Quaternary Sci Rev*, **22**, 1169–76

Berger, G W, 2003 Luminescence chronology of late Pleistocene loess-paleosol and tephra sequences near Fairbanks, Alaska, *Quaternary Res*, **60**, 70–83

Berger, G W, Mulhern, P J, and Huntley, D J, 1980 Isolation of silt-sized quartz from sediments, *Ancient TL*, **11**, 147–52

Bøtter-Jensen, L, Mejdahl, V, and Murray, A S, 1999 New light on OSL, *Quaternary Sci Rev*, **18**, 303–10

Bøtter-Jensen, L, McKeever, S W S, and Wintle, A G, 2003 *Optically Stimulated Luminescence Dosimetry*, Amsterdam (Elsevier)

Duller, G A T, 2003 Distinguishing quartz and feldspar in single grain luminescence measurements, *Radiation Measurements*, **37**, 161–5

Earle, S, 2009 'Testing the chronostratigraphy of the River Severn's terraces using optically stimulated luminescence dating', unpubl BSc thesis, Univ of Gloucestershire

Galbraith, R F, 1990 The radial plot: graphical assessment of spread in ages, *Nuclear Tracks and Radiation Measurements*, **17**, 207–14

Galbraith, R F, Roberts, R G, Laslett, G M, Yoshida, H, and Olley, J M, 1999 Optical dating of single and multiple grains of quartz from Jinmium rock shelter (northern Australia): Part I, Experimental design and statistical models, *Archaeometry*, **41**, 339–64

Hubble, J H, 1982 Photon mass attenuation and energy-absorption coefficients from 1keV to 20MeV, *Int J Applied Radioisotopes*, **33**, 1269–90

Huntley, D J, Godfrey-Smith, D I, and Thewalt, M L W, 1985 Optical dating of sediments, *Nature*, **313**, 105–7

Hütt, G, Jaek, I, and Tchonka, J, 1988 Optical dating: K-feldspars optical response stimulation spectra, *Quaternary Sci Rev*, **7**, 381–6

Jackson, M L, Sayin, M, and Clayton, R N, 1976 Hexafluorosilicic acid regent modification for quartz isolation. *Soil Science Society of America Journal*, **40**, 958–60

Markey, B G, Bøtter-Jensen, L, and Duller, G A T, 1997 A new flexible system for measuring thermally and optically stimulated luminescence, *Radiation Measurements*, **27**, 83–9

Mejdahl, V, 1979 Thermoluminescence dating: beta-dose attenuation in quartz grains, *Archaeometry*, **21**, 61–72

Murray, A S, and Olley, J M, 2002 Precision and accuracy in the Optically Stimulated Luminescence dating of sedimentary quartz: a status review, *Geochronometria*, **21**, 1–16

Murray, A S, and Wintle, A G, 2000 Luminescence dating of quartz using an improved single-aliquot regenerative-dose protocol, *Radiation Measurements*, **32**, 57–73

Murray, A S, and Wintle, A G, 2003 The single aliquot regenerative dose protocol: potential for improvements in reliability, *Radiation Measurements*, **37**, 377–81

Murray, A S, Olley, J M, and Caitcheon, G G, 1995 Measurement of equivalent doses in quartz from contemporary water-lain sediments using optically stimulated luminescence, *Quaternary Sci Rev*, **14**, 365–71

Murray, A S, Wintle, A G, and Wallinga, J, 2002 Dose estimation using quartz OSL in the non-linear region of the growth curve, *Radiation Protection Dosimetry*, **101**, 371–4

Olley, J M, Murray, A S, and Roberts, R G, 1996 The effects of disequilibria in the Uranium and Thorium decay chains on burial dose rates in fluvial sediments, *Quaternary Sci Rev*, **15**, 751–60

Olley, J M, Caitcheon, G G, and Murray, A S, 1998 The distribution of apparent dose as determined by optically stimulated luminescence in small aliquots of fluvial quartz: implications for dating young sediments, *Quaternary Sci Rev*, **17**, 1033–40

Olley, J M, Caitcheon, G G, and Roberts R G, 1999 The origin of dose distributions in fluvial sediments, and the prospect of dating single grains from fluvial deposits using - optically stimulated luminescence, *Radiation Measurements*, **30,** 207–17

Olley, J M, Pietsch, T, and Roberts, R G, 2004 Optical dating of Holocene sediments from a variety of geomorphic settings using single grains of quartz, *Geomorphology*, **60**, 337–58

Pawley, S M, Toms, P S, Armitage, S J, Rose, J, 2010 Quartz luminescence dating of Anglian Stage fluvial sediments: Comparison of SAR age estimates to the terrace chronology of the Middle Thames valley, UK, *Quaternary Geochron*, **5**, 569–82

Prescott, J R, and Hutton, J T, 1994 Cosmic ray contributions to dose rates for luminescence and ESR dating: large depths and long-term time variations, *Radiation Measurements*, **23**, 497–500

Singhvi, A K, Bluszcz, A, Bateman, M D, Someshwar Rao, M, 2001 Luminescence dating of loess-palaeosol sequences and coversands: methodological aspects and palaeoclimatic implications, *Earth Sci Rev*, **54**, 193–211

Smith, B W, Rhodes, E J, Stokes, S, Spooner, N A, 1990 The optical dating of sediments using quartz, *Radiation Protection Dosimetry*, **34**, 75–8

Spooner, N A, 1993 'The validity of optical dating based on feldspar', unpubl DPhil thesis, Oxford Univ

Templer, R H, 1985 The removal of anomalous fading in zircons, *Nuclear Tracks and Radiation Measurements*, **10**, 531–7

Toms, P S, Brown, A G, Basell, L S, and Hosfield, R T, 2008 Palaeolithic Rivers of South-West Britain: Optically Stimulated Luminescence Dating of Residual Deposits of the Proto-Axe, Exe, Otter, and Doniford, *EH Res Dept Rep Ser*, **2/2008**

Toms, P S, Hosfield, R T, Chambers, J C, Green, C P, and Marshall, P, 2005 Optical dating of the Broom Palaeolithic sites, Devon and Dorest, *EH CfA Rep*, **16/2005**

Wallinga, J, 2002 Optically stimulated luminescence dating of fluvial deposits: a review, *Boreas*, **31**, 303–22

Wintle, A G, 1973 Anomalous fading of thermoluminescence in mineral samples, *Nature*, **245**, 143–4

Zimmerman, D W, 1971 Thermoluminescent dating using fine grains from pottery, *Archaeometry*, **13**, 29–52

TABLES

Field Code		CLIF04	CLIF03	CLIF01
Lab Code		GL08060	GL08059	GL08057
Location		52°N, 2°W, 10m	52°N, 2°W, 10m	52°N, 2°W, 10m
Overburden (m)		0.5	1.7	5.0
Grain size (μm)		5–15	125–180	125–180
Moisture content (%)		18 ± 5	16 ± 4	8 ± 2
NaI γ-spectrometry (in situ)	K (%)	1.48 ± 0.03	0.84 ± 0.02	0.98 ± 0.02
	Th (ppm)	8.26 ± 0.26	3.89 ± 0.19	3.43 ± 0.18
	U (ppm)	3.49 ± 0.17	1.90 ± 0.13	1.57 ± 0.12
γ D_r ($Gy.ka^{-1}$)		1.15 ± 0.04	0.60 ± 0.03	0.58 ± 0.02
Ge γ-spectrometry (lab based)	K (%)	2.32 ± 0.10	1.41 ± 0.07	1.22 ± 0.06
	Th (ppm)	11.69 ± 0.70	5.44 ± 0.41	3.89 ± 0.36
	U (ppm)	2.35 ± 0.13	1.24 ± 0.08	0.89 ± 0.07
α D_r ($Gy.ka^{-1}$)		0.44 ± 0.05	-	-
β D_r ($Gy.ka^{-1}$)		1.88 ± 0.19	1.03 ± 0.11	1.00 ± 0.08
Cosmic D_r ($Gy.ka^{-1}$)		0.19 ± 0.02	0.16 ± 0.01	0.09 ± 0.01
Total D_r ($Gy.ka^{-1}$)		3.66 ± 0.20	1.79 ± 0.11	1.67 ± 0.08
Preheat (°C for 10s)		200	240	220
De (Gy)		2.9 ± 0.1	4.4 ± 0.5	11.0 ± 1.6
Age (ka)		0.78 ± 0.06 (0.05)	2.5 ± 0.3 (0.3)	6.6 ± 1.0 (0.9)

Table 1: D_r, D_e and Age data of submitted samples. Uncertainties in age are quoted at 1σ confidence, are based on analytical errors and reflect combined systematic and experimental variability and (in parentheses) experimental variability alone (see 7.0). Blue indicates samples with accepted age estimates; red, age estimates with caveats (see Table 2)

Field Code		CLIF05	CLIF06	CLIF07
Lab Code		GL10021	GL10022	GL10023
Location		52°N, 2°W, 10m	52°N, 2°W, 10m	52°N, 2°W, 10m
Overburden (m)		3.5	3.5	3.0
Grain size (μm)		125-180	180-250	125-180
Moisture content (%)		5 ± 1	4 ± 1	8 ± 2
NaI γ-spectrometry (in situ)	K (%)	0.88 ± 0.02	0.86 ± 0.02	1.17 ± 0.02
	Th (ppm)	2.48 ± 0.15	2.13 ± 0.12	4.02 ± 0.15
	U (ppm)	0.98 ± 0.09	1.25 ± 0.09	2.35 ± 0.10
γ D_r ($Gy.ka^{-1}$)		0.44 ± 0.02	0.45 ± 0.02	0.74 ± 0.03
Ge γ-spectrometry (lab based)	K (%)	1.16 ± 0.06	1.18 ± 0.06	1.30 ± 0.06
	Th (ppm)	2.54 ± 0.30	2.42 ± 0.31	4.12 ± 0.39
	U (ppm)	0.60 ± 0.06	0.66 ± 0.06	0.87 ± 0.07
α D_r ($Gy.ka^{-1}$)		-	-	-
β D_r ($Gy.ka^{-1}$)		0.93 ± 0.07	0.94 ± 0.07	1.05 ± 0.08
Cosmic D_r ($Gy.ka^{-1}$)		0.12 ± 0.01	0.12 ± 0.01	0.13 ± 0.01
Total D_r ($Gy.ka^{-1}$)		1.49 ± 0.08	1.51 ± 0.08	1.92 ± 0.09
Preheat (°C for 10s)		240	240	260
De (Gy)		24.6 ± 2.4	22.9 ± 2.1	22.8 ± 3.7
Age (ka)		16 ± 2 (2)	15 ± 2 (1)	12 ± 2 (2)

Table 1 (cont): D_r, D_e and Age data of submitted samples. Uncertainties in age are quoted at 1 σ confidence, are based on analytical errors and reflect combined systematic and experimental variability and (in parentheses) experimental variability alone (see 7.0). Blue indicates samples with accepted age estimates; red, age estimates with caveats (see Table 2)

Field Code		FRAM01	FRAM02	BMIL01
Lab Code		GL10017	GL10018	GL10024
Location		52°N, 2°W, 20m	52°N, 2°W, 20m	52°N, 2°W, 30m
Overburden (m)		0.9	0.9	0.7
Grain size (μm)		125-180	125-180	125-180
Moisture content (%)		11 ± 3	11 ± 3	16 ± 4
NaI γ-spectrometry (in situ)	K (%)	0.17 ± 0.01	0.19 ± 0.01	1.00 ± 0.02
	Th (ppm)	1.49 ± 0.11	1.23 ± 0.10	3.73 ± 0.16
	U (ppm)	1.41 ± 0.09	1.30 ± 0.08	1.85 ± 0.11
γ D_r ($Gy.ka^{-1}$)		0.27 ± 0.01	0.25 ± 0.01	0.63 ± 0.02
Ge γ-spectrometry (lab based)	K (%)	0.54 ± 0.03	0.53 ± 0.03	1.48 ± 0.07
	Th (ppm)	2.02 ± 0.26	1.69 ± 0.30	7.10 ± 0.48
	U (ppm)	0.72 ± 0.06	0.64 ± 0.06	1.45 ± 0.09
α D_r ($Gy.ka^{-1}$)		-	-	-
β D_r ($Gy.ka^{-1}$)		0.46 ± 0.04	0.44 ± 0.04	1.17 ± 0.11
Cosmic D_r ($Gy.ka^{-1}$)		0.18 ± 0.02	0.18 ± 0.02	0.18 ± 0.02
Total D_r ($Gy.ka^{-1}$)		0.91 ± 0.05	0.87 ± 0.05	1.98 ± 0.11
Preheat (°C for 10s)		240	240	260
De (Gy)		16.4 ± 6.1	8.5 ± 0.9	181.3 ± 25.9
Age (ka)		18 ± 7 (7)	9.7 ± 1.2 (1.1)	92 ± 14 (13)

Table 1 (cont): D_r, D_e and Age data of submitted samples. Uncertainties in age are quoted at 1 σ confidence, are based on analytical errors and reflect combined systematic and experimental variability and (in parentheses) experimental variability alone (see 7.0). Blue indicates samples with accepted age estimates; red, age estimates with caveats (see Table 2)

Field Code		BMIL02	BMIL04	BMIL03
Lab Code		GL10025	GL10027	GL10026
Location		52°N, 2°W, 30m	52°N, 2°W, 30m	52°N, 2°W, 30m
Overburden (m)		1.0	4.5	2.0
Grain size (μm)		125-180	125-180	180-250
Moisture content		8 ± 2	5 ± 1	14 ± 4
NaI γ-spectrometry (in situ)	K (%)	0.93 ± 0.02	0.94 ± 0.02	0.91 ± 0.02
	Th (ppm)	2.42 ± 0.14	1.93 ± 0.12	2.61 ± 0.13
	U (ppm)	1.42 ± 0.10	0.95 ± 0.08	1.49 ± 0.09
γ D_r (Gy.ka^{-1})		0.50 ± 0.02	0.43 ± 0.02	0.51 ± 0.02
Ge γ-spectrometry (lab based)	K (%)	1.34 ± 0.06	1.11 ± 0.05	1.05 ± 0.05
	Th (ppm)	2.79 ± 0.27	2.68 ± 0.31	2.48 ± 0.33
	U (ppm)	0.70 ± 0.06	0.62 ± 0.06	0.59 ± 0.06
α D_r (Gy.ka^{-1})		-	-	-
β D_r (Gy.ka^{-1})		1.04 ± 0.08	0.90 ± 0.07	0.73 ± 0.07
Cosmic D_r (Gy.ka^{-1})		0.18 ± 0.01	0.10 ± 0.01	0.15 ± 0.01
Total D_r (Gy.ka^{-1})		1.71 ± 0.09	1.43 ± 0.07	1.40 ± 0.08
Preheat (°C for 10s)		280	280	280
De (Gy)		161.6 ± 22.1	118.8 ± 16.7	151.3 ± 18.2
Age (ka)		94 ± 14 (13)	83 ± 12 (12)	108 ± 14 (13)

Table 1 (cont): D_r, D_e and Age data of submitted samples. Uncertainties in age are quoted at 1 σ confidence, are based on analytical errors and reflect combined systematic and experimental variability and (in parentheses) experimental variability alone (see 7.0). Blue indicates samples with accepted age estimates; red, age estimates with caveats (see Table 2)

Generic considerations	Field Code	Lab Code	Sample-specific considerations
None	CLIF04	GL08060	Accept
	CLIF03	GL08059	Partially bleached (see 4.2.1; Appendix II, Fig. 7) Accept as maximum age
	CLIF01	GL08057	Partially bleached (see 4.2.1; Appendix III, Fig. 7) Accept as maximum age
	CLIF05	GL10021	Overdispersion of regenerative-dose data (see 4.1.4; Appendix IV, Fig. 5) Partially bleached (see 4.2.1; Appendix IV, Fig. 7) Accept tentatively as maximum age
	CLIF06	GL10022	Overdispersion of regenerative-dose data (see 4.1.4; Appendix V, Fig. 5) Minor U disequilibrium (see 5.0; Appendix V, Fig. 8) Accept tentatively
	CLIF07	GL10023	Overdispersion of regenerative-dose data (see 4.1.4; Appendix VI, Fig. 5) Accept tentatively
	FRAM01	GL10017	Partially bleached (see 4.2.1; Appendix VII, Fig. 7) Accept as maximum age
	FRAM02	GL10018	Overdispersion of regenerative-dose data (see 4.1.4; Appendix VIII, Fig. 5) Accept tentatively
	BMIL01	GL10024	Overdispersion of regenerative-dose data (see 4.1.4; Appendix IX, Fig. 5) Accept tentatively
	BMIL02	GL10025	Overdispersion of regenerative-dose data (see 4.1.4; Appendix X, Fig. 5) Moderate U disequilibrium (see 5.0; Appendix X, Fig. 8) Accept tentatively
	BMIL04	GL10027	Overdispersion of regenerative-dose data (see 4.1.4; Appendix XI, Fig. 5) Accept tentatively
	BMIL03	GL10026	Overdispersion of regenerative-dose data (see 4.1.4; Appendix XII, Fig. 5) Moderate U disequilibrium (see 5.0; Appendix XII, Fig. 8) Accept tentatively

Table 2: Validity of sample suite age estimates and caveats for consideration

FIGURES

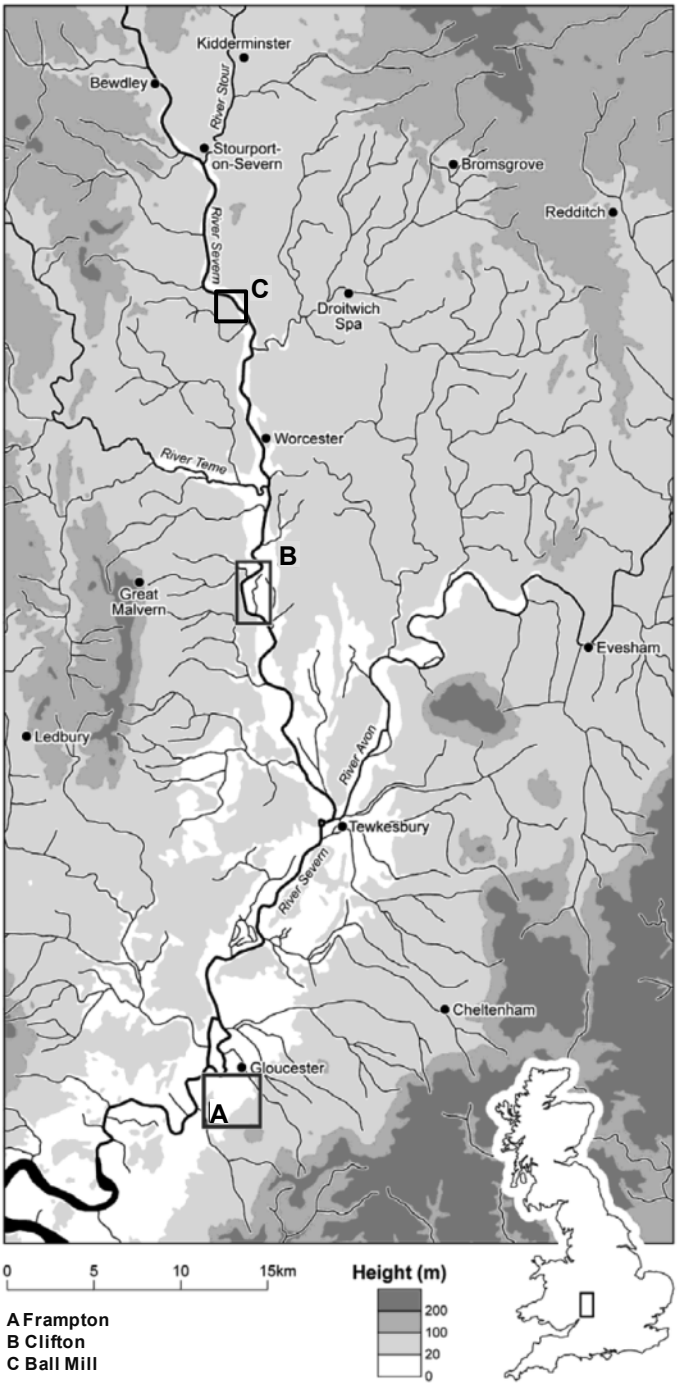

Figure 1: Location of study sites

Figure 2: Optical dating samples from Frampton, Gloucestershire (51°45'28.58"N, 2°20'26.60"W)

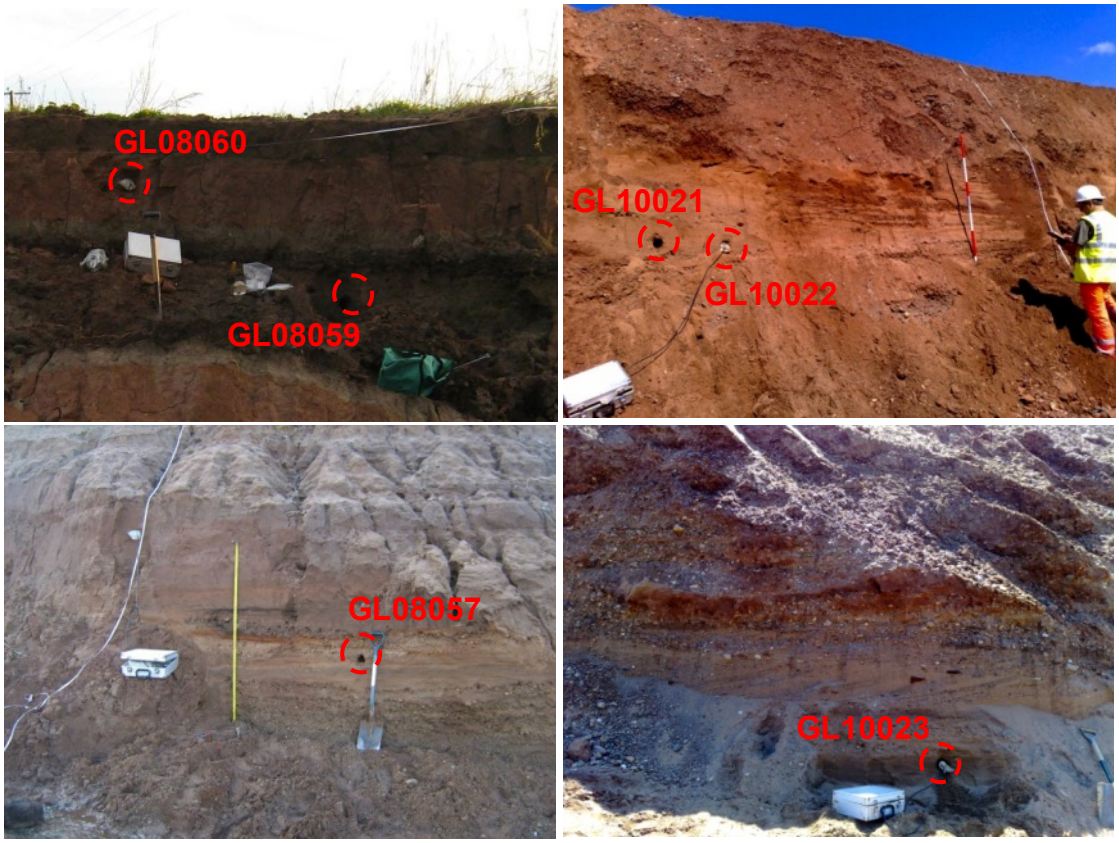

Figure 3: Optical dating samples from Clifton, Worcestershire (GL08 057, 059 and 060 52°45'28.58"N, 2°13'43.40"W; GL10 021 and 022 52°07'10.01"N, 2°13'28.53"W; GL10023 52°07'11.19"N, 2°13'31.19"W)

Figure 4: Optical dating samples from Ball Mill, Worcestershire (52°15'02.39"N, 2°15'09.15"W)

APPENDIX 1: TECHNICAL DATA FOR SAMPLE GL08060

Fig. 1 Signal Calibration

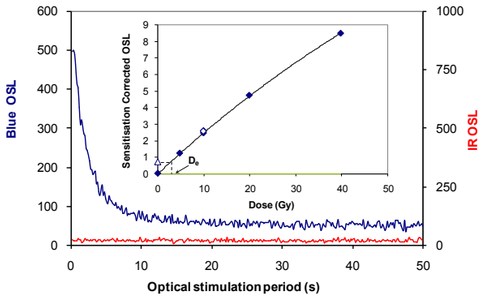

Fig. 1 Signal Calibration Natural blue and laboratory-induced infrared (IR) OSL signals. Detectable IR signal decays are diagnostic of feldspar contamination. Inset, the natural blue OSL signal (open triangle) of each aliquot is calibrated against known laboratory doses to yield equivalent dose (D_e) values. Repeats of low and high doses (open diamonds) illustrate the success of sensitivity correction.

Fig. 2 D_e Preheat Dependence The acquisition of D_e values is necessarily predicated upon thermal treatment of aliquots succeeding environmental and laboratory irradiation. The D_e preheat dependence test quantifies the combined effects of thermal transfer and sensitisation on the natural signal. Insignificant adjustment in D_e may reflect limited influence of these effects.

Fig. 3 Dose Recovery Attempts to replicate the above diagnostic, yet provide improved resolution of thermal effects through removal of variability induced by heterogeneous dose absorption in the environment and using a precise lab dose to simulate natural dose. Based on this and D_e preheat dependence data an appropriate thermal treatment is selected to refine the final D_e value.

Fig. 4 Inter-aliquot D_e distribution Provides a measure of inter-aliquot statistical concordance in D_e values derived from **natural** irradiation. Discordant data (those points lying beyond **±2 standardised ln D_e**) reflects heterogeneous dose absorption and/or inaccuracies in calibration.

Fig. 5 Low and High Repeat Regenerative-dose Ratio Measures the statistical concordance of signals from repeated low and high regenerative-doses. Discordant data (those points lying beyond **±2 standardised ln D_e**) indicate inaccurate sensitivity correction.

Fig. 6 OSL to Post-IR OSL Ratio Measures the statistical concordance of OSL and post-IR OSL responses to the same regenerative-dose. Discordant, underestimating data (those points lying below **-2 standardised ln D_e**) highlight the presence of significant feldspar contamination.

Fig. 7 Signal Analysis Statistically significant increase in **natural** D_e value with signal stimulation period is indicative of a partially-bleached signal, provided a significant increase in D_e results from **simulated partial bleaching** followed by insignificant adjustment in D_e for simulated **zero** and **full bleach** conditions. Ages from such samples are considered maximum estimates. In the absence of a significant rise in D_e with stimulation time, simulated partial bleaching and zero/full bleach tests are not assessed.

Fig. 8 U Activity Statistical concordance (**equilibrium**) in the activities of the daughter radioisotope ^{226}Ra with its parent ^{238}U may signify the temporal stability of D_r emissions from these chains. Significant differences (disequilibrium; **>50%**) in activity indicate addition or removal of isotopes creating a time-dependent shift in D_r values and increased uncertainty in the accuracy of age estimates. A **20%** disequilibrium marker is also shown.

Fig. 9 Age Range The **mean age range** provides an estimate of sediment burial period based on mean D_e and D_r values with associated analytical uncertainties. The **probability distribution** indicates the inter-aliquot variability in age. The **maximum influence** of temporal variations in D_r forced by minima-maxima variation in moisture content and overburden thickness may prove instructive where there is uncertainty in these parameters, however the combined extremes represented should not be construed as preferred age estimates.

Fig. 2 D_e Preheat Dependence

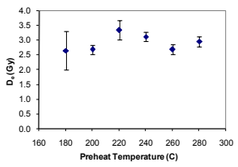

Fig. 3 Dose Recovery

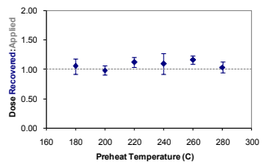

Fig. 4 Inter-aliquot D_e distribution

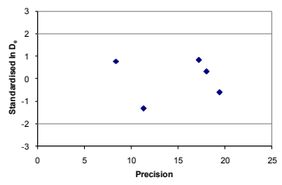

Fig. 5 Low and High Repeat Regenerative-dose Ratio

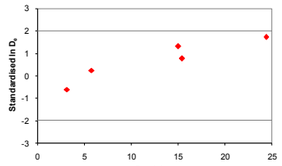

Fig. 6 OSL to Post-IR OSL Ratio

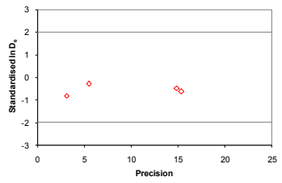

Sample: GL08060

Fig. 7 Signal Analysis

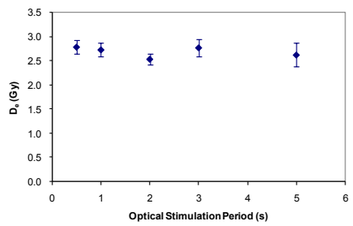

Fig. 8 U Decay Activity

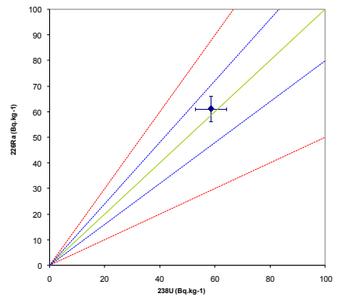

Fig. 9 Age Range

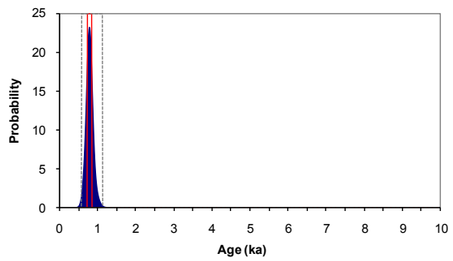

APPENDIX 11: TECHNICAL DATA FOR SAMPLE GL08059

Fig. 1 Signal Calibration

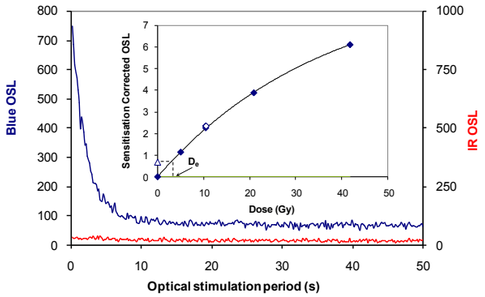

Fig. 1 Signal Calibration Natural blue and laboratory-induced infrared (IR) OSL signals. Detectable IR signal decays are diagnostic of feldspar contamination. Inset, the natural blue OSL signal (open triangle) of each aliquot is calibrated against known laboratory doses to yield equivalent dose (D_e) values. Repeats of low and high doses (open diamonds) illustrate the success of sensitivity correction.

Fig. 2 D_e Preheat Dependence The acquisition of D_e values is necessarily predicated upon thermal treatment of aliquots succeeding environmental and laboratory irradiation. The D_e preheat dependence test quantifies the combined effects of thermal transfer and sensitisation on the natural signal. Insignificant adjustment in D_e may reflect limited influence of these effects.

Fig. 3 Dose Recovery Attempts to replicate the above diagnostic, yet provide improved resolution of thermal effects through removal of variability induced by heterogeneous dose absorption in the environment and using a precise lab dose to simulate natural dose. Based on this and D_e preheat dependence data an appropriate thermal treatment is selected to refine the final D_e value.

Fig. 4 Inter-aliquot D_e distribution Provides a measure of inter-aliquot statistical concordance in D_e values derived from **natural** irradiation. Discordant data (those points lying beyond **±2 standardised ln D_e**) reflects heterogeneous dose absorption and/or inaccuracies in calibration.

Fig. 5 Low and High Repeat Regenerative-dose Ratio Measures the statistical concordance of signals from repeated low and high regenerative-doses. Discordant data (those points lying beyond **±2 standardised ln D_e**) indicate inaccurate sensitivity correction.

Fig. 6 OSL to Post-IR OSL Ratio Measures the statistical concordance of OSL and post-IR OSL responses to the same regenerative-dose. Discordant, underestimating data (those points lying below **-2 standardised ln D_e**) highlight the presence of significant feldspar contamination.

Fig. 7 Signal Analysis Statistically significant increase in **natural** D_e value with signal stimulation period is indicative of a partially-bleached signal, provided a significant increase in D_e results from **simulated partial bleaching** followed by insignificant adjustment in D_e for simulated **zero** and **full bleach** conditions. Ages from such samples are considered maximum estimates. In the absence of a significant rise in D_e with stimulation time, simulated partial bleaching and zero/full bleach tests are not assessed.

Fig. 8 U Activity Statistical concordance (**equilibrium**) in the activities of the daughter radioisotope ^{226}Ra with its parent ^{238}U may signify the temporal stability of D_r emissions from these chains. Significant differences (disequilibrium; **>50%**) in activity indicate addition or removal of isotopes creating a time-dependent shift in D_r values and increased uncertainty in the accuracy of age estimates. A **20%** disequilibrium marker is also shown.

Fig. 9 Age Range The **mean age range** provides an estimate of sediment burial period based on mean D_e and D_r values with associated analytical uncertainties. The **probability distribution** indicates the inter-aliquot variability in age. The **maximum influence** of temporal variations in D_r forced by minima-maxima variation in moisture content and overburden thickness may prove instructive where there is uncertainty in these parameters, however the combined extremes represented should not be construed as preferred age estimates.

Fig. 2 D_e Preheat Dependence

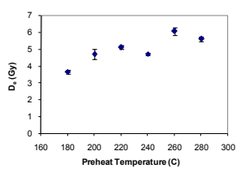

Fig. 3 Dose Recovery

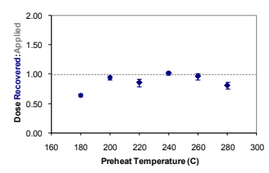

Fig. 4 Inter-aliquot D_e distribution

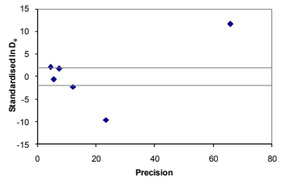

Fig. 5 Low and High Repeat Regenerative-dose Ratio

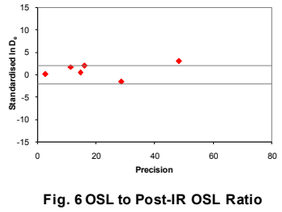

Fig. 6 OSL to Post-IR OSL Ratio

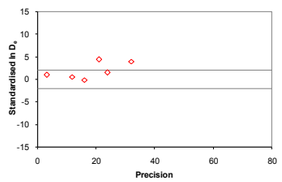

Sample: GL08059

Fig. 7 Signal Analysis

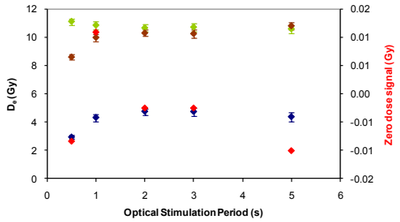

Fig. 8 U Decay Activity

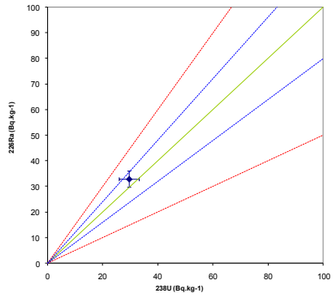

Fig. 9 Age Range

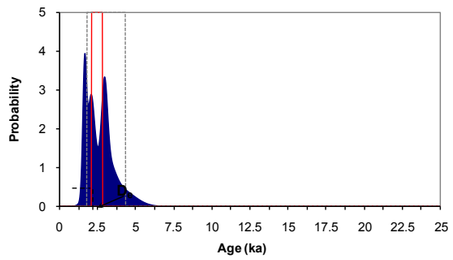

APPENDIX III: TECHNICAL DATA FOR SAMPLE GL08057

Fig. 1 Signal Calibration

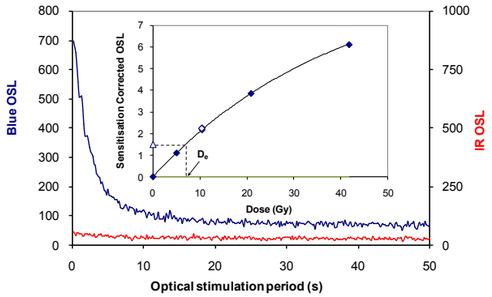

Fig. 1 Signal Calibration Natural blue and laboratory-induced infrared (IR) OSL signals. Detectable IR signal decays are diagnostic of feldspar contamination. Inset, the natural blue OSL signal (open triangle) of each aliquot is calibrated against known laboratory doses to yield equivalent dose (D_e) values. Repeats of low and high doses (open diamonds) illustrate the success of sensitivity correction.

Fig. 2 D_e Preheat Dependence The acquisition of D_e values is necessarily predicated upon thermal treatment of aliquots succeeding environmental and laboratory irradiation. The D_e preheat dependence test quantifies the combined effects of thermal transfer and sensitisation on the natural signal. Insignificant adjustment in D_e may reflect limited influence of these effects.

Fig. 3 Dose Recovery Attempts to replicate the above diagnostic, yet provide improved resolution of thermal effects through removal of variability induced by heterogeneous dose absorption in the environment and using a precise lab dose to simulate natural dose. Based on this and D_e preheat dependence data an appropriate thermal treatment is selected to refine the final D_e value.

Fig. 4 Inter-aliquot D_e distribution Provides a measure of inter-aliquot statistical concordance in D_e values derived from **natural** irradiation. Discordant data (those points lying beyond **±2 standardised ln D_e**) reflects heterogeneous dose absorption and/or inaccuracies in calibration.

Fig. 5 Low and High Repeat Regenerative-dose Ratio Measures the statistical concordance of signals from repeated low and high regenerative-doses. Discordant data (those points lying beyond **±2 standardised ln D_e**) indicate inaccurate sensitivity correction.

Fig. 6 OSL to Post-IR OSL Ratio Measures the statistical concordance of OSL and post-IR OSL responses to the same regenerative-dose. Discordant, underestimating data (those points lying below **-2 standardised ln D_e**) highlight the presence of significant feldspar contamination.

Fig. 7 Signal Analysis Statistically significant increase in **natural** D_e value with signal stimulation period is indicative of a partially-bleached signal, provided a significant increase in D_e results from **simulated partial bleaching** followed by insignificant adjustment in D_e for simulated **zero** and **full bleach** conditions. Ages from such samples are considered maximum estimates. In the absence of a significant rise in D_e with stimulation time, simulated partial bleaching and zero/full bleach tests are not assessed.

Fig. 8 U Activity Statistical concordance (equilibrium) in the activities of the daughter radioisotope ^{226}Ra with its parent ^{238}U may signify the temporal stability of D_r emissions from these chains. Significant differences (disequilibrium; >50%) in activity indicate addition or removal of isotopes creating a time-dependent shift in D_r values and increased uncertainty in the accuracy of age estimates. A 20% disequilibrium marker is also shown.

Fig. 9 Age Range The **mean age range** provides an estimate of sediment burial period based on mean D_e and D_r values with associated analytical uncertainties. The probability distribution indicates the inter-aliquot variability in age. The **maximum influence** of temporal variations in D_r forced by minima-maxima variation in moisture content and overburden thickness may prove instructive where there is uncertainty in these parameters, however the combined extremes represented should not be construed as preferred age estimates.

Fig. 2 D_e Preheat Dependence

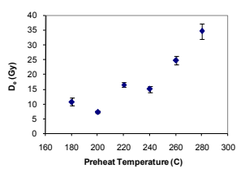

Fig. 3 Dose Recovery

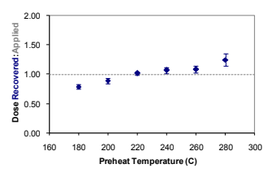

Fig. 4 Inter-aliquot D_e distribution

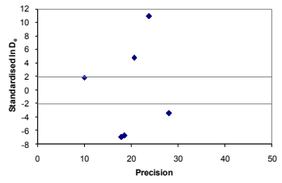

Fig. 5 Low and High Repeat Regenerative-dose Ratio

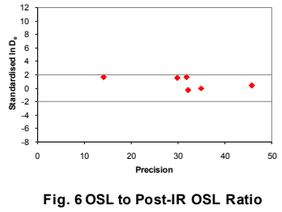

Fig. 6 OSL to Post-IR OSL Ratio

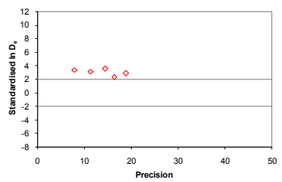

Sample: GL08057

Fig. 7 Signal Analysis

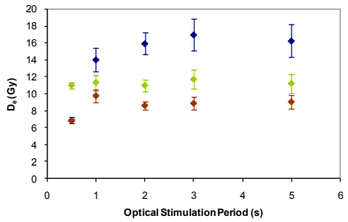

Fig. 8 U Decay Activity

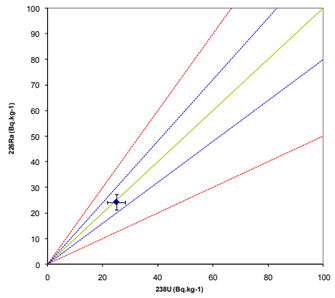

Fig. 9 Age Range

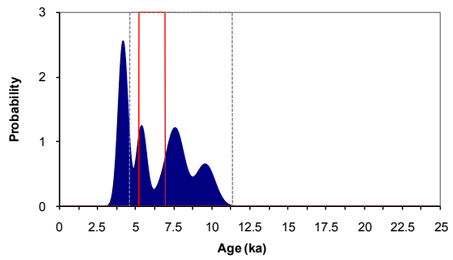

APPENDIX 1V: TECHNICAL DATA FOR SAMPLE GL10021

Fig. 1 Signal Calibration

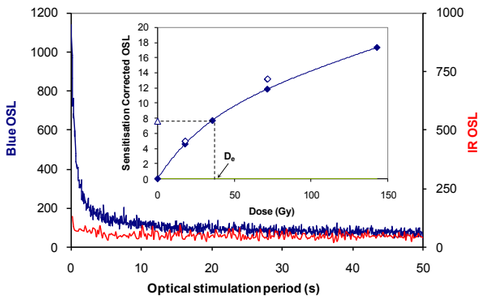

Fig. 1 Signal Calibration Natural blue and laboratory-induced infrared (IR) OSL signals. Detectable IR signal decays are diagnostic of feldspar contamination. Inset, the natural blue OSL signal (open triangle) of each aliquot is calibrated against known laboratory doses to yield equivalent dose (D_e) values. Repeats of low and high doses (open diamonds) illustate the success of sensitivity correction.

Fig. 2 D_e Preheat Dependence The acquisition of D_e values is necessarily predicated upon thermal treatment of aliquots succeeding environmental and laboratory irradiation. The D_e preheat dependence test quantifies the combined effects of thermal transfer and sensitisation on the natural signal. Insignificant adjustment in D_e may reflect limited influence of these effects.

Fig. 3 Dose Recovery Attempts to replicate the above diagnostic, yet provide improved resolution of thermal effects through removal of variability induced by heterogeneous dose absoption in the environment and using a precise lab dose to simulate natural dose. Based on this and D_e preheat dependence data an appropriate thermal treatment is selected to refine the final D_e value.

Fig. 4 Inter-aliquot D_e distribution Provides a measure of inter-aliquot statistical concordance in D_e values derived from **natural** irradiation. Discordant data (those points lying beyond ±2 standardised ln D_e) reflects heterogeneous dose absorption and/or inaccuracies in calibration.

Fig. 5 Low and High Repeat Regenerative-dose Ratio Measures the statistical concordance of signals from repeated low and high regenerative-doses. Discordant data (those points lying beyond ±2 standardised ln D_e) indicate inaccurate sensitivity correction.

Fig. 6 OSL to Post-IR OSL Ratio Measures the statistical concordance of OSL and post-IR OSL responses to the same regenerative-dose. Discordant, underestimating data (those points lying below -2 standardised ln D_e) highlight the presence of significant feldspar contamination.

Fig. 7 Signal Analysis Statistically significant increase in **natural** D_e value with signal stimulation period is indicative of a partially-bleached signal, provided a significant increase in D_e results from **simulated partial bleaching** followed by insignificant adjustment in D_e for simulated **zero** and **full bleach** conditions. Ages from such samples are considered maximum estimates. In the absence of a significant rise in D_e with stimulation time, simulated partial bleaching and zero/full bleach tests are not assessed.

Fig. 8 U Activity Statistical concordance (equilibrium) in the activities of the daughter radioisotope ^{226}Ra with its parent ^{238}U may signify the temporal stability of D_r emissions from these chains. Significant differences (disequilibrium; >50%) in activity indicate addition or removal of isotopes creating a time-dependent shift in D_r values and increased uncertainty in the accuracy of age estimates. A 20% disequilibrium marker is also shown.

Fig. 9 Age Range The **mean age range** provides an estimate of sediment burial period based on mean D_e and D_r values with associated analytical uncertainties. The probability distribution indicates the inter-aliquot variability in age. The **maximum influence** of temporal variations in D_r forced by minima-maxima variation in moisture content and overburden thickness may prove instructive where there is uncertainty in these parameters, however the combined extremes represented should not be construed as preferred age estimates.

Fig. 2 D_e Preheat Dependence

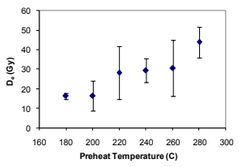

Fig. 3 Dose Recovery

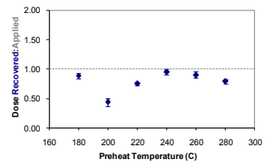

Fig. 4 Inter-aliquot D_e distribution

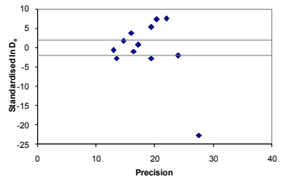

Fig. 5 Low and High Repeat Regenerative-dose Ratio

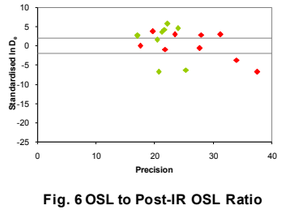

Fig. 6 OSL to Post-IR OSL Ratio

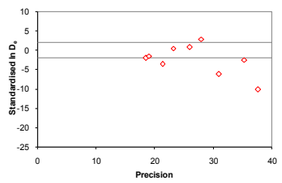

Sample: GL10021

Fig. 7 Signal Analysis

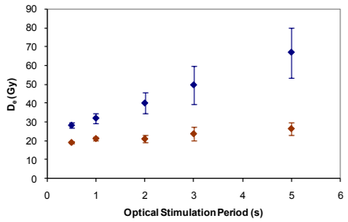

Fig. 8 U Decay Activity

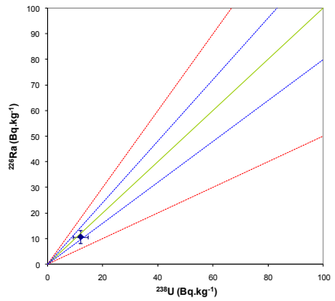

Fig. 9 Age Range

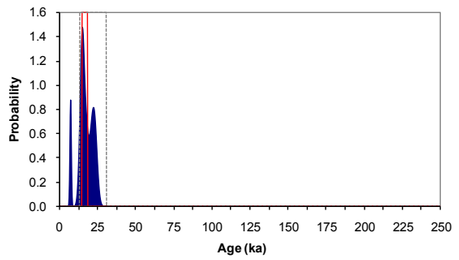

APPENDIX V: TECHNICAL DATA FOR SAMPLE GL10022

Fig. 1 Signal Calibration

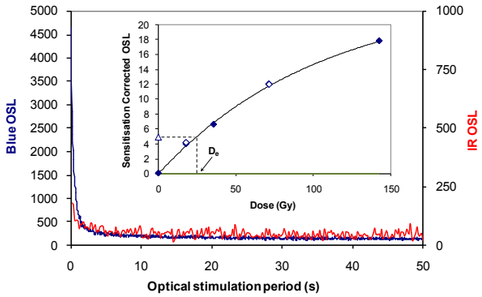

Fig. 1 Signal Calibration Natural blue and laboratory-induced infrared (IR) OSL signals. Detectable IR signal decays are diagnostic of feldspar contamination. Inset, the natural blue OSL signal (open triangle) of each aliquot is calibrated against known laboratory doses to yield equivalent dose (D_e) values. Repeats of low and high doses (open diamonds) illustrate the success of sensitivity correction.

Fig. 2 D_e Preheat Dependence The acquisition of D_e values is necessarily predicated upon thermal treatment of aliquots succeeding environmental and laboratory irradiation. The D_e preheat dependence test quantifies the combined effects of thermal transfer and sensitisation on the natural signal. Insignificant adjustment in D_e may reflect limited influence of these effects.

Fig. 3 Dose Recovery Attempts to replicate the above diagnostic, yet provide improved resolution of thermal effects through removal of variability induced by heterogeneous dose absorption in the environment and using a precise lab dose to simulate natural dose. Based on this and D_e preheat dependence data an appropriate thermal treatment is selected to refine the final D_e value.

Fig. 4 Inter-aliquot D_e distribution Provides a measure of inter-aliquot statistical concordance in D_e values derived from **natural** irradiation. Discordant data (those points lying beyond ±2 standardised ln D_e) reflects heterogeneous dose absorption and/or inaccuracies in calibration.

Fig. 5 Low and High Repeat Regenerative-dose Ratio Measures the statistical concordance of signals from repeated low and high regenerative-doses. Discordant data (those points lying beyond ±2 standardised ln D_e) indicate inaccurate sensitivity correction.

Fig. 6 OSL to Post-IR OSL Ratio Measures the statistical concordance of OSL and post-IR OSL responses to the same regenerative-dose. Discordant, underestimating data (those points lying below -2 standardised ln D_e) highlight the presence of significant feldspar contamination.

Fig. 7 Signal Analysis Statistically significant increase in **natural** D_e value with signal stimulation period is indicative of a partially-bleached signal, provided a significant increase in D_e results from **simulated partial bleaching** followed by insignificant adjustment in D_e for simulated **zero** and **full bleach** conditions. Ages from such samples are considered maximum estimates. In the absence of a significant rise in D_e with stimulation time, simulated partial bleaching and zero/full bleach tests are not assessed.

Fig. 8 U Activity Statistical concordance (equilibrium) in the activities of the daughter radioisotope ^{226}Ra with its parent ^{238}U may signify the temporal stability of D_r emissions from these chains. Significant differences (disequilibrium; >50%) in activity indicate addition or removal of isotopes creating a time-dependent shift in D_r values and increased uncertainty in the accuracy of age estimates. A 20% disequilibrium marker is also shown.

Fig. 9 Age Range The **mean age range** provides an estimate of sediment burial period based on mean D_e and D_r values with associated analytical uncertainties. The probability distribution indicates the inter-aliquot variability in age. The **maximum influence** of temporal variations in D_r forced by minima-maxima variation in moisture content and overburden thickness may prove instructive where there is uncertainty in these parameters, however the combined extremes represented should not be construed as preferred age estimates.

Fig. 2 D_e Preheat Dependence

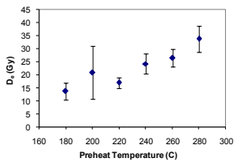

Fig. 3 Dose Recovery

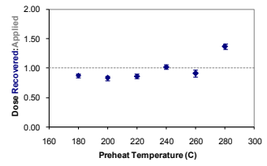

Fig. 4 Inter-aliquot D_e distribution

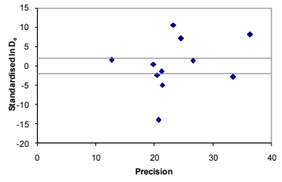

Fig. 5 Low and High Repeat Regenerative-dose Ratio

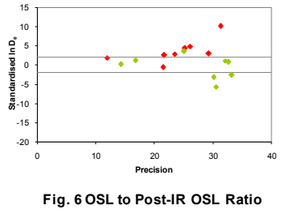

Fig. 6 OSL to Post-IR OSL Ratio

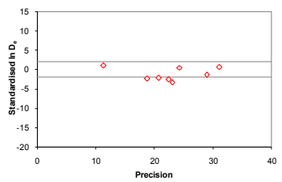

Sample: GL10022

Fig. 7 Signal Analysis

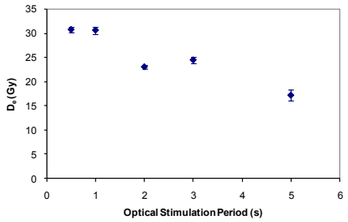

Fig. 8 U Decay Activity

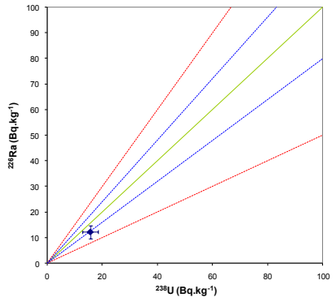

Fig. 9 Age Range

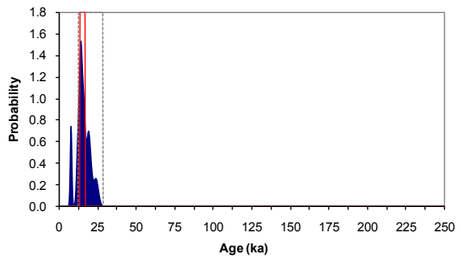

APPENDIX VI: TECHNICAL DATA FOR SAMPLE GL10023

Fig. 1 Signal Calibration

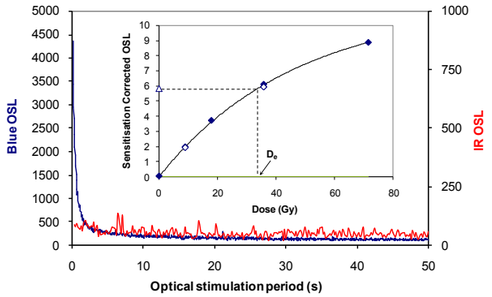

Fig. 1 Signal Calibration Natural blue and laboratory-induced infrared (IR) OSL signals. Detectable IR signal decays are diagnostic of feldspar contamination. Inset, the natural blue OSL signal (open triangle) of each aliquot is calibrated against known laboratory doses to yield equivalent dose (D_e) values. Repeats of low and high doses (open diamonds) illustrate the success of sensitivity correction.

Fig. 2 D_e Preheat Dependence The acquisition of D_e values is necessarily predicated upon thermal treatment of aliquots succeeding environmental and laboratory irradiation. The D_e preheat dependence test quantifies the combined effects of thermal transfer and sensitisation on the natural signal. Insignificant adjustment in D_e may reflect limited influence of these effects.

Fig. 3 Dose Recovery Attempts to replicate the above diagnostic, yet provide improved resolution of thermal effects through removal of variability induced by heterogeneous dose absorption in the environment and using a precise lab dose to simulate natural dose. Based on this and D_e preheat dependence data an appropriate thermal treatment is selected to refine the final D_e value.

Fig. 4 Inter-aliquot D_e distribution Provides a measure of inter-aliquot statistical concordance in D_e values derived from **natural** irradiation. Discordant data (those points lying beyond ±2 standardised ln D_e) reflects heterogeneous dose absorption and/or inaccuracies in calibration.

Fig. 5 Low and High Repeat Regenerative-dose Ratio Measures the statistical concordance of signals from repeated low and high regenerative-doses. Discordant data (those points lying beyond ±2 standardised ln D_e) indicate inaccurate sensitivity correction.

Fig. 6 OSL to Post-IR OSL Ratio Measures the statistical concordance of OSL and post-IR OSL responses to the same regenerative-dose. Discordant, underestimating data (those points lying below -2 standardised ln D_e) highlight the presence of significant feldspar contamination.

Fig. 7 Signal Analysis Statistically significant increase in **natural** D_e value with signal stimulation period is indicative of a partially-bleached signal, provided a significant increase in D_e results from **simulated partial bleaching** followed by insignificant adjustment in D_e for simulated **zero** and **full bleach** conditions. Ages from such samples are considered maximum estimates. In the absence of a significant rise in D_e with stimulation time, simulated partial bleaching and zero/full bleach tests are not assessed.

Fig. 8 U Activity Statistical concordance (equilibrium) in the activities of the daughter radioisotope ^{226}Ra with its parent ^{238}U may signify the temporal stability of D_r emissions from these chains. Significant differences (disequilibrium; >50%) in activity indicate addition or removal of isotopes creating a time-dependent shift in D_r values and increased uncertainty in the accuracy of age estimates. A 20% disequilibrium marker is also shown.

Fig. 9 Age Range The **mean age range** provides an estimate of sediment burial period based on mean D_e and D_r values with associated analytical uncertainties. The probability distribution indicates the inter-aliquot variability in age. The **maximum influence** of temporal variations in D_r forced by minima-maxima variation in moisture content and overburden thickness may prove instructive where there is uncertainty in these parameters, however the combined extremes represented should not be construed as preferred age estimates.

Fig. 2 D_e Preheat Dependence

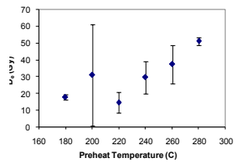

Fig. 3 Dose Recovery

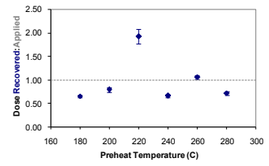

Fig. 4 Inter-aliquot D_e distribution

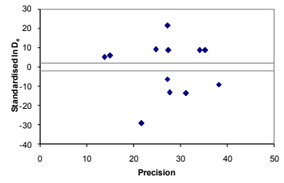

Fig. 5 Low and High Repeat Regenerative-dose Ratio

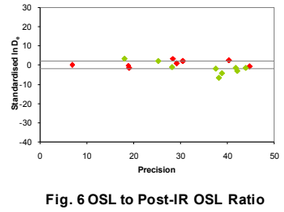

Fig. 6 OSL to Post-IR OSL Ratio

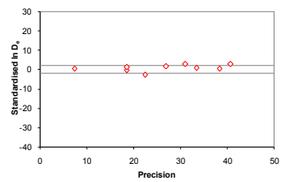

Sample: GL10023

Fig. 7 Signal Analysis

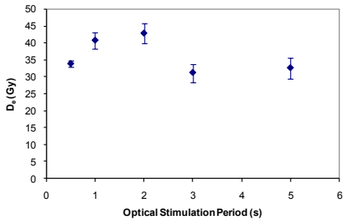

Fig. 8 U Decay Activity

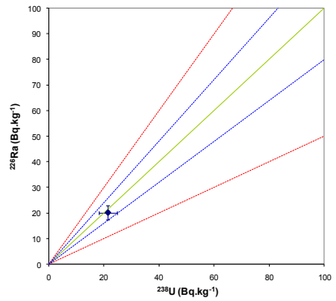

Fig. 9 Age Range

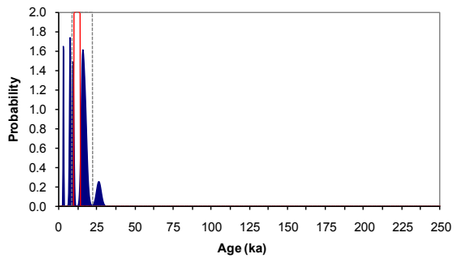

APPENDIX VII: TECHNICAL DATA FOR SAMPLE GL10017

Fig. 1 Signal Calibration

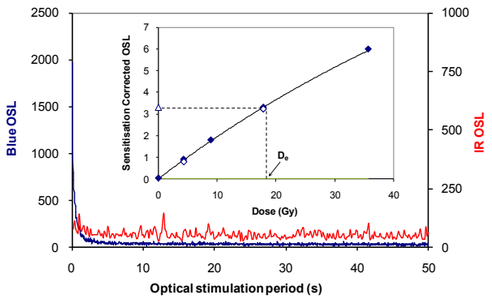

Fig. 1 Signal Calibration Natural blue and laboratory-induced infrared (IR) OSL signals. Detectable IR signal decays are diagnostic of feldspar contamination. Inset, the natural blue OSL signal (open triangle) of each aliquot is calibrated against known laboratory doses to yield equivalent dose (D_e) values. Repeats of low and high doses (open diamonds) illustrate the success of sensitivity correction.

Fig. 2 D_e Preheat Dependence The acquisition of D_e values is necessarily predicated upon thermal treatment of aliquots succeeding environmental and laboratory irradiation. The D_e preheat dependence test quantifies the combined effects of thermal transfer and sensitisation on the natural signal. Insignificant adjustment in D_e may reflect limited influence of these effects.

Fig. 3 Dose Recovery Attempts to replicate the above diagnostic, yet provide improved resolution of thermal effects through removal of variability induced by heterogeneous dose absorption in the environment and using a precise lab dose to simulate natural dose. Based on this and D_e preheat dependence data an appropriate thermal treatment is selected to refine the final D_e value.

Fig. 4 Inter-aliquot D_e distribution Provides a measure of inter-aliquot statistical concordance in D_e values derived from **natural** irradiation. Discordant data (those points lying beyond ±2 standardised ln D_e) reflects heterogeneous dose absorption and/or inaccuracies in calibration.

Fig. 5 Low and High Repeat Regenerative-dose Ratio Measures the statistical concordance of signals from repeated low and high regenerative-doses. Discordant data (those points lying beyond ±2 standardised ln D_e) indicate inaccurate sensitivity correction.

Fig. 6 OSL to Post-IR OSL Ratio Measures the statistical concordance of OSL and post-IR OSL responses to the same regenerative-dose. Discordant, underestimating data (those points lying below -2 standardised ln D_e) highlight the presence of significant feldspar contamination.

Fig. 7 Signal Analysis Statistically significant increase in **natural** D_e value with signal stimulation period is indicative of a partially-bleached signal, provided a significant increase in D_e results from **simulated partial bleaching** followed by insignificant adjustment in D_e for simulated **zero** and **full bleach** conditions. Ages from such samples are considered maximum estimates. In the absence of a significant rise in D_e with stimulation time, simulated partial bleaching and zero/full bleach tests are not assessed.

Fig. 8 U Activity Statistical concordance (equilibrium) in the activities of the daughter radioisotope ^{226}Ra with its parent ^{238}U may signify the temporal stability of D_r emissions from these chains. Significant differences (disequilibrium; >50%) in activity indicate addition or removal of isotopes creating a time-dependent shift in D_r values and increased uncertainty in the accuracy of age estimates. A 20% disequilibrium marker is also shown.

Fig. 9 Age Range The **mean age range** provides an estimate of sediment burial period based on mean D_e and D_r values with associated analytical uncertainties. The probability distribution indicates the inter-aliquot variability in age. The **maximum influence** of temporal variations in D_r forced by minima-maxima variation in moisture content and overburden thickness may prove instructive where there is uncertainty in these parameters, however the combined extremes represented should not be construed as preferred age estimates.

Fig. 2 D_e Preheat Dependence

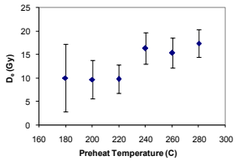

Fig. 3 Dose Recovery

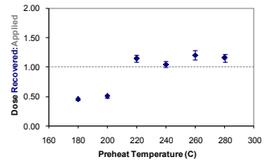

Fig. 4 Inter-aliquot D_e distribution

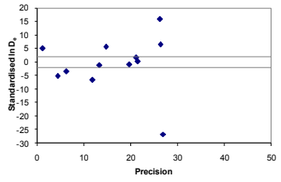

Fig. 5 Low and High Repeat Regenerative-dose Ratio

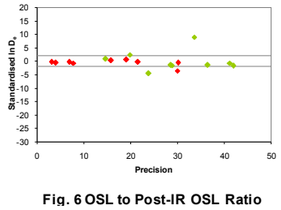

Fig. 6 OSL to Post-IR OSL Ratio

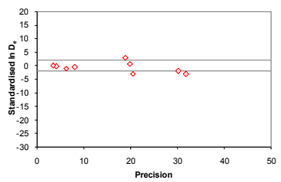

Sample: GL10017

Fig. 7 Signal Analysis

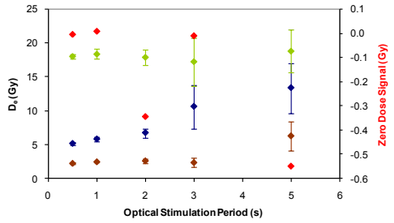

Fig. 8 U Decay Activity

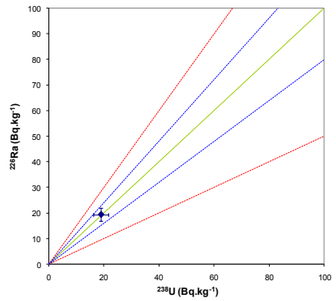

Fig. 9 Age Range

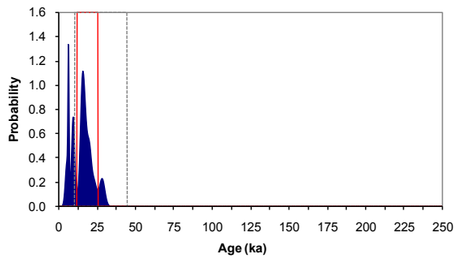

APPENDIX VIII: TECHNICAL DATA FOR SAMPLE GL10018

Fig. 1 Signal Calibration

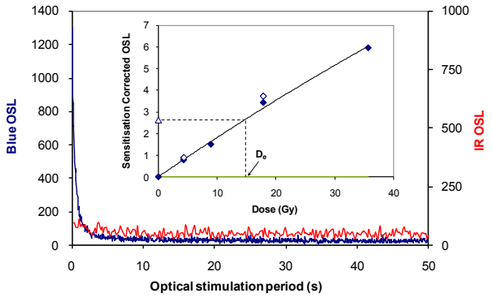

Fig. 1 Signal Calibration Natural blue and laboratory-induced infrared (IR) OSL signals. Detectable IR signal decays are diagnostic of feldspar contamination. Inset, the natural blue OSL signal (open triangle) of each aliquot is calibrated against known laboratory doses to yield equivalent dose (D_e) values. Repeats of low and high doses (open diamonds) illustrate the success of sensitivity correction.

Fig. 2 D_e Preheat Dependence The acquisition of D_e values is necessarily predicated upon thermal treatment of aliquots succeeding environmental and laboratory irradiation. The D_e preheat dependence test quantifies the combined effects of thermal transfer and sensitisation on the natural signal. Insignificant adjustment in D_e may reflect limited influence of these effects.

Fig. 3 Dose Recovery Attempts to replicate the above diagnostic, yet provide improved resolution of thermal effects through removal of variability induced by heterogeneous dose absorption in the environment and using a precise lab dose to simulate natural dose. Based on this and D_e preheat dependence data an appropriate thermal treatment is selected to refine the final D_e value.

Fig. 4 Inter-aliquot D_e distribution Provides a measure of inter-aliquot statistical concordance in D_e values derived from **natural** irradiation. Discordant data (those points lying beyond ±2 standardised ln D_e) reflects heterogeneous dose absorption and/or inaccuracies in calibration.

Fig. 5 Low and High Repeat Regenerative-dose Ratio Measures the statistical concordance of signals from repeated low and high regenerative-doses. Discordant data (those points lying beyond ±2 standardised ln D_e) indicate inaccurate sensitivity correction.

Fig. 6 OSL to Post-IR OSL Ratio Measures the statistical concordance of OSL and post-IR OSL responses to the same regenerative-dose. Discordant, underestimating data (those points lying below -2 standardised ln D_e) highlight the presence of significant feldspar contamination.

Fig. 7 Signal Analysis Statistically significant increase in **natural** D_e value with signal stimulation period is indicative of a partially-bleached signal, provided a significant increase in D_e results from **simulated partial bleaching** followed by insignificant adjustment in D_e for simulated **zero** and **full bleach** conditions. Ages from such samples are considered maximum estimates. In the absence of a significant rise in D_e with stimulation time, simulated partial bleaching and zero/full bleach tests are not assessed.

Fig. 8 U Activity Statistical concordance (equilibrium) in the activities of the daughter radioisotope ^{226}Ra with its parent ^{238}U may signify the temporal stability of D_r emissions from these chains. Significant differences (disequilibrium; >50%) in activity indicate addition or removal of isotopes creating a time-dependent shift in D_r values and increased uncertainty in the accuracy of age estimates. A 20% disequilibrium marker is also shown.

Fig. 9 Age Range The **mean age range** provides an estimate of sediment burial period based on mean D_e and D_r values with associated analytical uncertainties. The probability distribution indicates the inter-aliquot variability in age. The **maximum influence** of temporal variations in D_r forced by minima-maxima variation in moisture content and overburden thickness may prove instructive where there is uncertainty in these parameters, however the combined extremes represented should not be construed as preferred age estimates.

Fig. 2 D_e Preheat Dependence

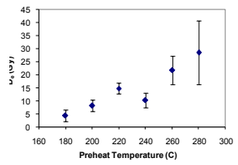

Fig. 3 Dose Recovery

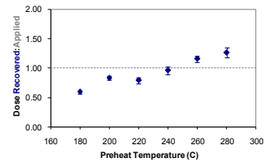

Fig. 4 Inter-aliquot D_e distribution

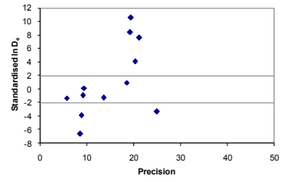

Fig. 5 Low and High Repeat Regenerative-dose Ratio

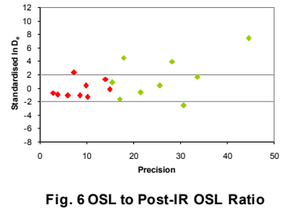

Fig. 6 OSL to Post-IR OSL Ratio

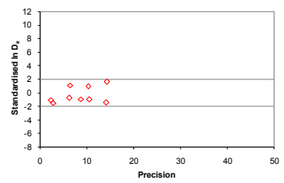

Sample: GL10018

Fig. 7 Signal Analysis

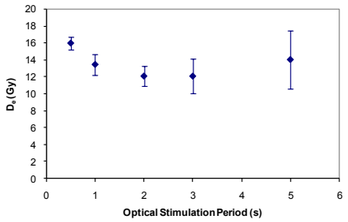

Fig. 8 U Decay Activity

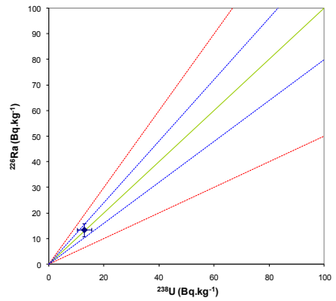

Fig. 9 Age Range

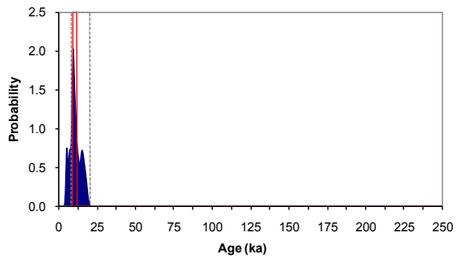

APPENDIX IX: TECHNICAL DATA FOR SAMPLE GL10024

Fig. 1 Signal Calibration

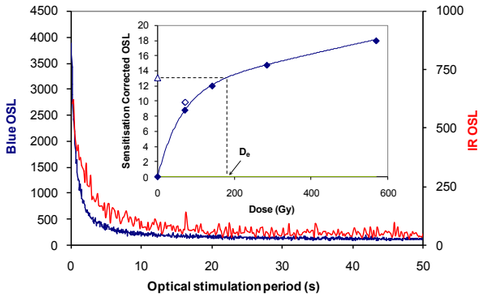

Fig. 1 Signal Calibration Natural blue and laboratory-induced infrared (IR) OSL signals. Detectable IR signal decays are diagnostic of feldspar contamination. Inset, the natural blue OSL signal (open triangle) of each aliquot is calibrated against known laboratory doses to yield equivalent dose (D_e) values. Repeats of low and high doses (open diamonds) illustrate the success of sensitivity correction.

Fig. 2 D_e Preheat Dependence The acquisition of D_e values is necessarily predicated upon thermal treatment of aliquots succeeding environmental and laboratory irradiation. The D_e preheat dependence test quantifies the combined effects of thermal transfer and sensitisation on the natural signal. Insignificant adjustment in D_e may reflect limited influence of these effects.

Fig. 3 Dose Recovery Attempts to replicate the above diagnostic, yet provide improved resolution of thermal effects through removal of variability induced by heterogeneous dose absorption in the environment and using a precise lab dose to simulate natural dose. Based on this and D_e preheat dependence data an appropriate thermal treatment is selected to refine the final D_e value.

Fig. 4 Inter-aliquot D_e distribution Provides a measure of inter-aliquot statistical concordance in D_e values derived from **natural** irradiation. Discordant data (those points lying beyond ±2 standardised ln D_e) reflects heterogeneous dose absorption and/or inaccuracies in calibration.

Fig. 5 Low and High Repeat Regenerative-dose Ratio Measures the statistical concordance of signals from repeated low and high regenerative-doses. Discordant data (those points lying beyond ±2 standardised ln D_e) indicate inaccurate sensitivity correction.

Fig. 6 OSL to Post-IR OSL Ratio Measures the statistical concordance of OSL and post-IR OSL responses to the same regenerative-dose. Discordant, underestimating data (those points lying below -2 standardised ln D_e) highlight the presence of significant feldspar contamination.

Fig. 7 Signal Analysis Statistically significant increase in **natural** D_e value with signal stimulation period is indicative of a partially-bleached signal, provided a significant increase in D_e results from **simulated partial bleaching** followed by insignificant adjustment in D_e for simulated **zero** and **full bleach** conditions. Ages from such samples are considered maximum estimates. In the absence of a significant rise in D_e with stimulation time, simulated partial bleaching and zero/full bleach tests are not assessed.

Fig. 8 U Activity Statistical concordance (equilibrium) in the activities of the daughter radioisotope ^{226}Ra with its parent ^{238}U may signify the temporal stability of D_r emissions from these chains. Significant differences (disequilibrium; >50%) in activity indicate addition or removal of isotopes creating a time-dependent shift in D_r values and increased uncertainty in the accuracy of age estimates. A 20% disequilibrium marker is also shown.

Fig. 9 Age Range The **mean age range** provides an estimate of sediment burial period based on mean D_e and D_r values with associated analytical uncertainties. The probability distribution indicates the inter-aliquot variability in age. The **maximum influence** of temporal variations in D_r forced by minima-maxima variation in moisture content and overburden thickness may prove instructive where there is uncertainty in these parameters, however the combined extremes represented should not be construed as preferred age estimates.

Fig. 2 D_e Preheat Dependence

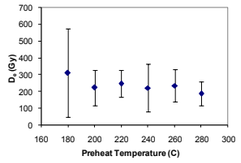

Fig. 3 Dose Recovery

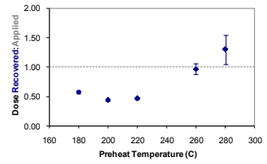

Fig. 4 Inter-aliquot D_e distribution

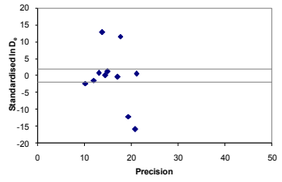

Fig. 5 Low and High Repeat Regenerative-dose Ratio

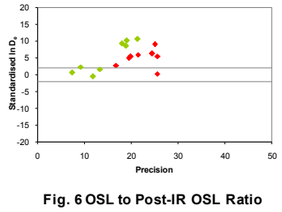

Fig. 6 OSL to Post-IR OSL Ratio

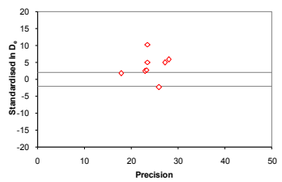

Sample: GL10024

Fig. 7 Signal Analysis

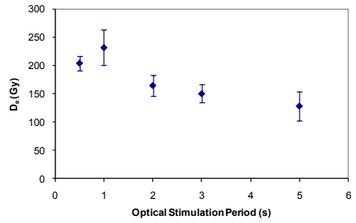

Fig. 8 U Decay Activity

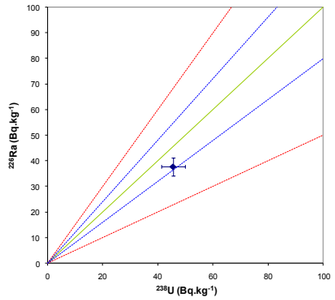

Fig. 9 Age Range

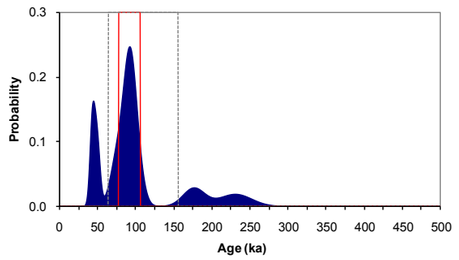

APPENDIX X: TECHNICAL DATA FOR SAMPLE GL10025

Fig. 1 Signal Calibration

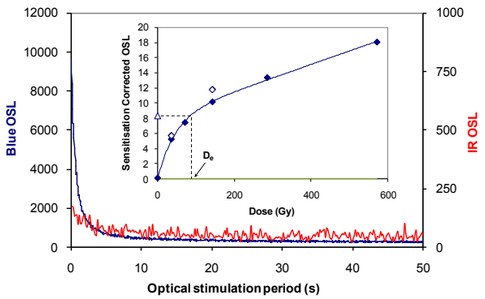

Fig. 1 Signal Calibration Natural blue and laboratory-induced infrared (IR) OSL signals. Detectable IR signal decays are diagnostic of feldspar contamination. Inset, the natural blue OSL signal (open triangle) of each aliquot is calibrated against known laboratory doses to yield equivalent dose (D_e) values. Repeats of low and high doses (open diamonds) illustrate the success of sensitivity correction.

Fig. 2 D_e Preheat Dependence The acquisition of D_e values is necessarily predicated upon thermal treatment of aliquots succeeding environmental and laboratory irradiation. The D_e preheat dependence test quantifies the combined effects of thermal transfer and sensitisation on the natural signal. Insignificant adjustment in D_e may reflect limited influence of these effects.

Fig. 3 Dose Recovery Attempts to replicate the above diagnostic, yet provide improved resolution of thermal effects through removal of variability induced by heterogeneous dose absorption in the environment and using a precise lab dose to simulate natural dose. Based on this and D_e preheat dependence data an appropriate thermal treatment is selected to refine the final D_e value.

Fig. 4 Inter-aliquot D_e distribution Provides a measure of inter-aliquot statistical concordance in D_e values derived from **natural** irradiation. Discordant data (those points lying beyond ±2 standardised ln D_e) reflects heterogeneous dose absorption and/or inaccuracies in calibration.

Fig. 5 Low and High Repeat Regenerative-dose Ratio Measures the statistical concordance of signals from repeated low and high regenerative-doses. Discordant data (those points lying beyond ±2 standardised ln D_e) indicate inaccurate sensitivity correction.

Fig. 6 OSL to Post-IR OSL Ratio Measures the statistical concordance of OSL and post-IR OSL responses to the same regenerative-dose. Discordant, underestimating data (those points lying below -2 standardised ln D_e) highlight the presence of significant feldspar contamination.

Fig. 7 Signal Analysis Statistically significant increase in **natural** D_e value with signal stimulation period is indicative of a partially-bleached signal, provided a significant increase in D_e results from **simulated partial bleaching** followed by insignificant adjustment in D_e for simulated **zero** and **full bleach** conditions. Ages from such samples are considered maximum estimates. In the absence of a significant rise in D_e with stimulation time, simulated partial bleaching and zero/full bleach tests are not assessed.

Fig. 8 U Activity Statistical concordance (equilibrium) in the activities of the daughter radioisotope ^{226}Ra with its parent ^{238}U may signify the temporal stability of D_r emissions from these chains. Significant differences (disequilibrium; >50%) in activity indicate addition or removal of isotopes creating a time-dependent shift in D_r values and increased uncertainty in the accuracy of age estimates. A 20% disequilibrium marker is also shown.

Fig. 9 Age Range The **mean age range** provides an estimate of sediment burial period based on mean D_e and D_r values with associated analytical uncertainties. The probability distribution indicates the inter-aliquot variability in age. The **maximum influence** of temporal variations in D_r forced by minima-maxima variation in moisture content and overburden thickness may prove instructive where there is uncertainty in these parameters, however the combined extremes represented should not be construed as preferred age estimates.

Fig. 2 D_e Preheat Dependence

Insufficient sample mass

Fig. 3 Dose Recovery

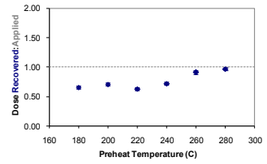

Fig. 4 Inter-aliquot D_e distribution

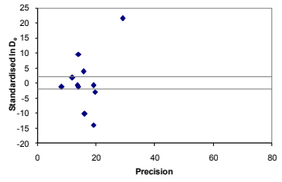

Fig. 5 Low and High Repeat Regenerative-dose Ratio

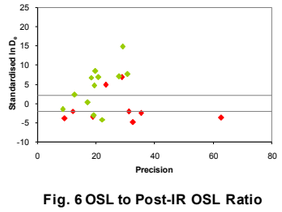

Fig. 6 OSL to Post-IR OSL Ratio

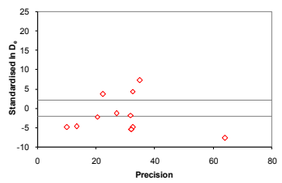

Sample: GL10025

Fig. 7 Signal Analysis

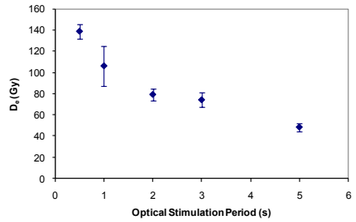

Fig. 8 U Decay Activity

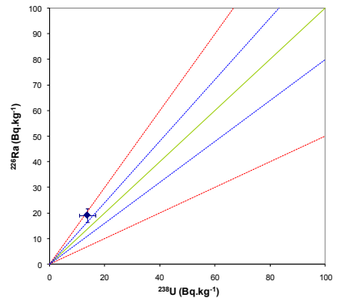

Fig. 9 Age Range

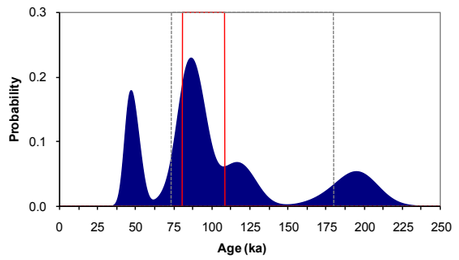

APPENDIX XI: TECHNICAL DATA FOR SAMPLE GL10027

Fig. 1 Signal Calibration

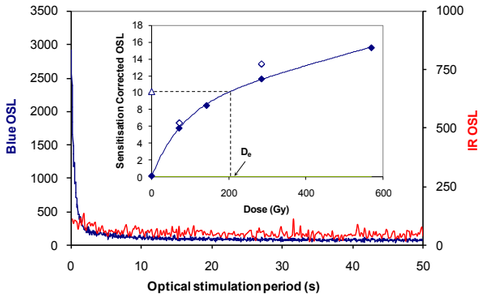

Fig. 1 Signal Calibration Natural blue and laboratory-induced infrared (IR) OSL signals. Detectable IR signal decays are diagnostic of feldspar contamination. Inset, the natural blue OSL signal (open triangle) of each aliquot is calibrated against known laboratory doses to yield equivalent dose (D_e) values. Repeats of low and high doses (open diamonds) illustrate the success of sensitivity correction.

Fig. 2 D_e Preheat Dependence The acquisition of D_e values is necessarily predicated upon thermal treatment of aliquots succeeding environmental and laboratory irradiation. The D_e preheat dependence test quantifies the combined effects of thermal transfer and sensitisation on the natural signal. Insignificant adjustment in D_e may reflect limited influence of these effects.

Fig. 3 Dose Recovery Attempts to replicate the above diagnostic, yet provide improved resolution of thermal effects through removal of variability induced by heterogeneous dose absorption in the environment and using a precise lab dose to simulate natural dose. Based on this and D_e preheat dependence data an appropriate thermal treatment is selected to refine the final D_e value.

Fig. 4 Inter-aliquot D_e distribution Provides a measure of inter-aliquot statistical concordance in D_e values derived from **natural** irradiation. Discordant data (those points lying beyond **±2 standardised ln D_e**) reflects heterogeneous dose absorption and/or inaccuracies in calibration.

Fig. 5 Low and High Repeat Regenerative-dose Ratio Measures the statistical concordance of signals from repeated low and high regenerative-doses. Discordant data (those points lying beyond **±2 standardised ln D_e**) indicate inaccurate sensitivity correction.

Fig. 6 OSL to Post-IR OSL Ratio Measures the statistical concordance of OSL and post-IR OSL responses to the same regenerative-dose. Discordant, underestimating data (those points lying below **-2 standardised ln D_e**) highlight the presence of significant feldspar contamination.

Fig. 7 Signal Analysis Statistically significant increase in **natural** D_e value with signal stimulation period is indicative of a partially-bleached signal, provided a significant increase in D_e results from **simulated partial bleaching** followed by insignificant adjustment in D_e for simulated **zero** and **full bleach** conditions. Ages from such samples are considered maximum estimates. In the absence of a significant rise in D_e with stimulation time, simulated partial bleaching and zero/full bleach tests are not assessed.

Fig. 8 U Activity Statistical concordance (**equilibrium**) in the activities of the daughter radioisotope ^{226}Ra with its parent ^{238}U may signify the temporal stability of D_r emissions from these chains. Significant differences (disequilibrium; **>50%**) in activity indicate addition or removal of isotopes creating a time-dependent shift in D_r values and increased uncertainty in the accuracy of age estimates. A **20%** disequilibrium marker is also shown.

Fig. 9 Age Range The **mean age range** provides an estimate of sediment burial period based on mean D_e and D_r values with associated analytical uncertainties. The **probability distribution** indicates the inter-aliquot variability in age. The **maximum influence** of temporal variations in D_r forced by minima-maxima variation in moisture content and overburden thickness may prove instructive where there is uncertainty in these parameters, however the combined extremes represented should not be construed as preferred age estimates.

Fig. 2 D_e Preheat Dependence

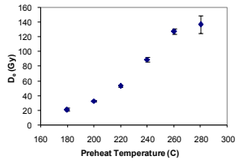

Fig. 3 Dose Recovery

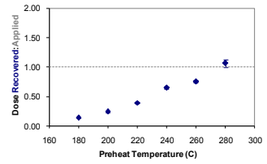

Fig. 4 Inter-aliquot D_e distribution

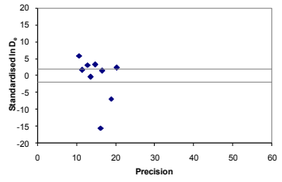

Fig. 5 Low and High Repeat Regenerative-dose Ratio

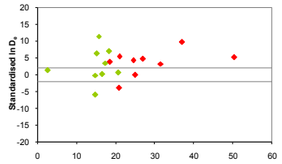

Fig. 6 OSL to Post-IR OSL Ratio

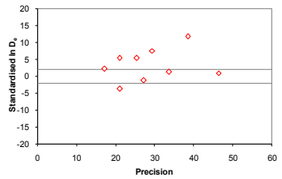

Sample: GL10027

Fig. 7 Signal Analysis

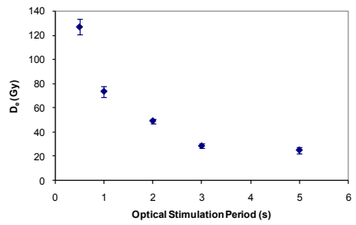

Fig. 8 U Decay Activity

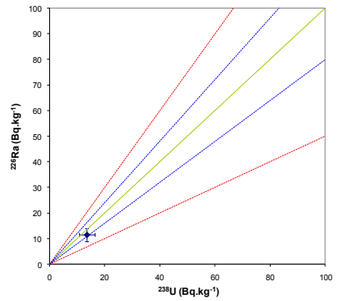

Fig. 9 Age Range

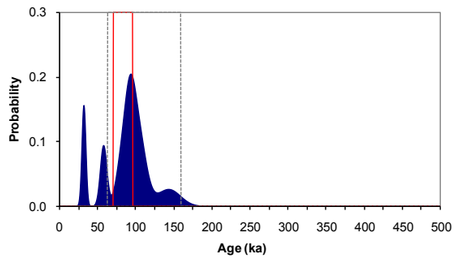

APPENDIX XII: TECHNICAL DATA FOR SAMPLE GL10026

Fig. 1 Signal Calibration

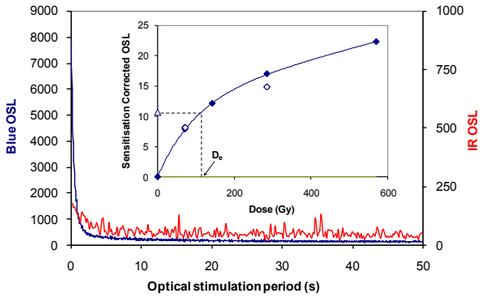

Fig. 1 Signal Calibration Natural blue and laboratory-induced infrared (IR) OSL signals. Detectable IR signal decays are diagnostic of feldspar contamination. Inset, the natural blue OSL signal (open triangle) of each aliquot is calibrated against known laboratory doses to yield equivalent dose (D_e) values. Repeats of low and high doses (open diamonds) illustrate the success of sensitivity correction.

Fig. 2 D_e Preheat Dependence The acquisition of D_e values is necessarily predicated upon thermal treatment of aliquots succeeding environmental and laboratory irradiation. The D_e preheat dependence test quantifies the combined effects of thermal transfer and sensitisation on the natural signal. Insignificant adjustment in D_e may reflect limited influence of these effects.

Fig. 3 Dose Recovery Attempts to replicate the above diagnostic, yet provide improved resolution of thermal effects through removal of variability induced by heterogeneous dose absorption in the environment and using a precise lab dose to simulate natural dose. Based on this and D_e preheat dependence data an appropriate thermal treatment is selected to refine the final D_e value.

Fig. 4 Inter-aliquot D_e distribution Provides a measure of inter-aliquot statistical concordance in D_e values derived from **natural** irradiation. Discordant data (those points lying beyond ±2 standardised ln D_e) reflects heterogeneous dose absorption and/or inaccuracies in calibration.

Fig. 5 Low and High Repeat Regenerative-dose Ratio Measures the statistical concordance of signals from repeated low and high regenerative-doses. Discordant data (those points lying beyond ±2 standardised ln D_e) indicate inaccurate sensitivity correction.

Fig. 6 OSL to Post-IR OSL Ratio Measures the statistical concordance of OSL and post-IR OSL responses to the same regenerative-dose. Discordant, underestimating data (those points lying below -2 standardised ln D_e) highlight the presence of significant feldspar contamination.

Fig. 7 Signal Analysis Statistically significant increase in **natural** D_e value with signal stimulation period is indicative of a partially-bleached signal, provided a significant increase in D_e results from **simulated partial bleaching** followed by insignificant adjustment in D_e for simulated **zero** and **full bleach** conditions. Ages from such samples are considered maximum estimates. In the absence of a significant rise in D_e with stimulation time, simulated partial bleaching and zero/full bleach tests are not assessed.

Fig. 8 U Activity Statistical concordance (equilibrium) in the activities of the daughter radioisotope ^{226}Ra with its parent ^{238}U may signify the temporal stability of D_r emissions from these chains. Significant differences (disequilibrium; >50%) in activity indicate addition or removal of isotopes creating a time-dependent shift in D_r values and increased uncertainty in the accuracy of age estimates. A 20% disequilibrium marker is also shown.

Fig. 9 Age Range The **mean age range** provides an estimate of sediment burial period based on mean D_e and D_r values with associated analytical uncertainties. The probability distribution indicates the inter-aliquot variability in age. The **maximum influence** of temporal variations in D_r forced by minima-maxima variation in moisture content and overburden thickness may prove instructive where there is uncertainty in these parameters, however the combined extremes represented should not be construed as preferred age estimates.

Fig. 2 D_e Preheat Dependence

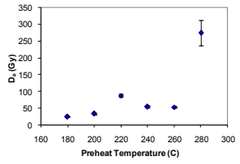

Fig. 3 Dose Recovery

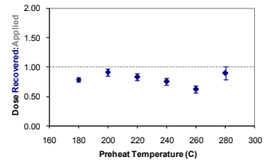

Fig. 4 Inter-aliquot D_e distribution

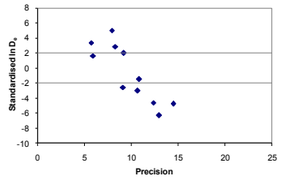

Fig. 5 Low and High Repeat Regenerative-dose Ratio

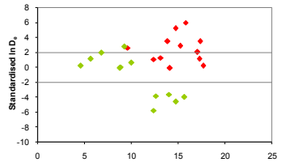

Fig. 6 OSL to Post-IR OSL Ratio

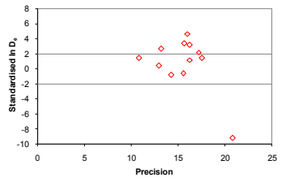

Sample: GL10026

Fig. 7 Signal Analysis

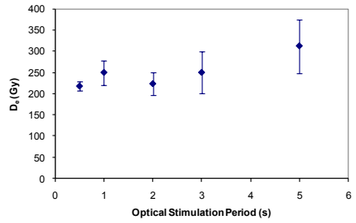

Fig. 8 U Decay Activity

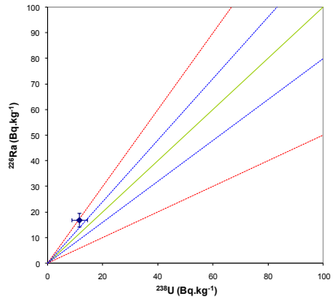

Fig. 9 Age Range

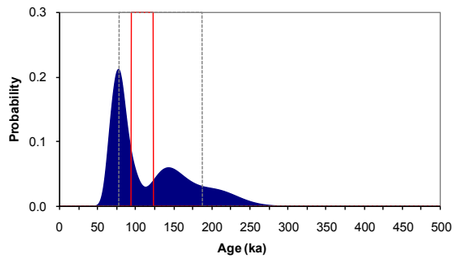






ENGLISH HERITAGE RESEARCH DEPARTMENT

English Heritage undertakes and commissions research into the historic environment, and the issues that affect its condition and survival, in order to provide the understanding necessary for informed policy and decision making, for sustainable management, and to promote the widest access, appreciation and enjoyment of our heritage.

The Research Department provides English Heritage with this capacity in the fields of buildings history, archaeology, and landscape history. It brings together seven teams with complementary investigative and analytical skills to provide integrated research expertise across the range of the historic environment. These are:

* *Aerial Survey and Investigation*
* *Archaeological Projects (excavation)*
* *Archaeological Science*
* *Archaeological Survey and Investigation (landscape analysis)*
* *Architectural Investigation*
* *Imaging, Graphics and Survey (including measured and metric survey, and photography)*
* *Survey of London*

The Research Department undertakes a wide range of investigative and analytical projects, and provides quality assurance and management support for externally-commissioned research. We aim for innovative work of the highest quality which will set agendas and standards for the historic environment sector. In support of this, and to build capacity and promote best practice in the sector, we also publish guidance and provide advice and training. We support outreach and education activities and build these in to our projects and programmes wherever possible.

We make the results of our work available through the Research Department Report Series, and through journal publications and monographs. Our publication Research News, which appears three times a year, aims to keep our partners within and outside English Heritage up-to-date with our projects and activities. A full list of Research Department Reports, with abstracts and information on how to obtain copies, may be found on www.english-heritage.org.uk/researchreports

For further information visit www.english-heritage.org.uk

ENGLISH HERITAGE